

CONTENTS

Sr. No.	TITLE	PAGE
1.	AMINO ACID ANALYSIS USING ION EXCHANGE RESINS A. S. KHAN AND F. FAIZ	01
2.	FUNDAMENTAL GROUP OF THE DYNAMICAL GRAPH M. El-Ghoul AND M. A. EL-FATTAH	19
3.	ON s^* -CLOSED SETS AND s^* -NORMAL SPACES M. KHAN, T. NOIRI AND M. HUSSAIN	31
4.	THE EFFECT OF FLUORINE DOPING ON OPTOELECTRONIC PROPERTIES OF TIN-DIOXIDE (F: SnO ₂) THIN FILMS S. A. YOUSAF AND S. ALI	43
5.	EFFECT OF PARTICLE SIZE ON THE STRUCTURAL AND TRANSPORT PROPERTIES OF La _{0.67} Ca _{0.33} MnO ₃ NANOPARTICLES M. Z. IQBAL, S. ALI AND M. A. MIRZA	51
6.	VARIATION OF ION ENERGY FLUX WITH INCREASING WORKING GAS PRESSURES USING FARADAY CUP IN PLASMA FOCUS DEVICE H. A. R. TARIQ, I. A. KHAN, U. IKHLAQ AND A. HUSSNAIN	65
7.	UNIAXIALLY STRAINED Si/SiGe HETEROSTRUCTURES A. R. KHAN	73
8.	X-RAY DIFFRACTION ANALYSIS OF Si/SiGe RESONANT TUNNELING STRUCTURES A. R. KHAN, M. MEDUÑA, G. BAUER, C. FALUB AND D. GRUETZMACHER	81

EDITORIAL BOARD

MANAGING EDITOR

R. Ahmad, Department of Physics,
Government College University, Lahore-54000, PAKISTAN
E-mail: jnsn@gcu.edu.pk
http://www.gcu.edu.pk/FullTextJour/JNSM_Phy/JNSM.htm

SECTION EDITORS

Chemistry:	M. S. Iqbal	(Editor)
Computer:	W. M. Qazi	(Editor)
Mathematics:	K. H. Dar S. Ahmad	(Editor) (Associate Editor)
Physics:	A. Shahbaz A. U. Khan	(Editor) (Associate Editor)

ADVISORY BOARD

Panel of Foreign Advisors

Panel of Local Advisors

J. Meng P. R. China	M. Zakullah QAU, Islamabad
K. P. Shum Hong Kong University, China (SAR)	M.A. Malik Hamdard Institute of Information Technology, Islamabad
N. Tsintsadze Institute of Physics, Tbitsi, Georgia	I.U. Khan GC University, Lahore
S.U. Khan Dhaka University, Bangladesh	N.A.D. Khattak Gomal University D.I. Khan
T. Kaladze Tbilisi State University, Georgia	K. Ahmad School of Computer Sciences, NCBA&E, Lahore
J.S. Pan IMRE Singapore	E. Sandhu School of Computer Sciences, NCBA&E, Lahore
P. Lee NTU Singapore	A.M. Mirza QAU, Islamabad

Pakistan: Rs 250

Annual Subscription
Foreign Countries: US\$ 40

Overseas Air Mail Charges: US\$ 10

**The Journal is published bi-annually
In April and October**

Published by:

Riaz Ahmad for Government College University, Lahore, Pakistan

Printed at:

Mithas Enterprises Press, Lahore

AMINO ACID ANALYSIS USING ION EXCHANGE RESINS

A. S. KHAN AND F. FAIZ

Department of Food, Agriculture and Chemical Technology, Karakorum International
University, Northern Areas, Gilgit, Pakistan

Corresponding Author: ahmad_kiu@yahoo.com

(Received: April 13, 2008)

ABSTRACT: Amino acids, their occurrence and importance in living beings, are described. Important areas of the application of amino acid analysis are outlined. Various procedures for the hydrolysis of proteins and for the amino acid analysis are described. Concise description of the historical developments in the amino acid analysis procedures using ion exchange resins is given. Results of the amino acid analysis of some of the Gliadin protein using ion exchange resins are presented. Chemistry of the Ninhydrin method of the amino acid quantitative estimation is described. Most recent uses of this technique in research are given in this review.

Keywords: Amino acids, occurrence and importance, composition of ion exchange resins, application of amino acid analyses, various hydrolysis methods, historical development, ninhydrin method of quantitative estimation.

1. INTRODUCTION

Amino acids (Fig.1) are biologically active substances, and a number of them are essential for living beings. Amino acids are found in living cells as well as in body fluids of higher animals, in amounts, which vary according to the tissue and particular amino acid.

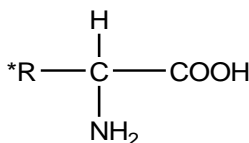


Fig. 1. General structural formula of amino acids (where R* can be H, CH₃, C(CH₃)₂ etc.)

In addition to the amino acids of proteins, a variety occurs free naturally. Some are metabolic products of the amino acids of proteins; for example α-aminobutyric acid occurs as the decarboxylation product of glutamic acid.

Others such as homoserine or ornithine are biosynthetic precursors of amino acids of proteins. Proteins on hydrolysis give amino acids, and their total number so far obtained appears to be twenty-five. All except two of them are α -amino acids; proline and hydroxyproline are amino acids (Table1). Ten of the amino acids are essential, and their deficiency prevents growth in young animals and may cause even death.

2. IMPORTANCE OF AMINO ACID ANALYSES

The techniques of amino acid analyses have gained paramount importance in biochemical research during the past two decades. There are three important fields of biochemical investigations in which it is routinely applied,

- 1) The investigation of the structure and composition of proteins particularly in the determination of their amino acid sequence.
- 2) The determination of amino acids in physiological fluids and tissues.
- 3) The determination of free amino acid composition of food stuffs to ascertain their food values.

Free amino acids can be estimated directly or after separation from the contaminating material by passing through ion exchange columns.

Table 1: Natural α amino acids (one amino group and one carboxylic group)

Name	Formula
Monoaminomonocarboxylic	
Glycine	$\text{CH}_2(\text{NH}_2)\text{COOH}$
Alanine	$\text{CH}_3\text{CH}(\text{NH}_2)\text{COOH}$
Valine	$(\text{CH}_3)_2\text{CHCH}(\text{NH}_2)\text{COOH}$
Leucine	$(\text{CH}_3)_2\text{CHCH}_2\text{CH}(\text{NH}_2)\text{COOH}$
Iso-Leucine	$\text{CH}_3\text{CH}_2\text{CH}(\text{CH}_3)\text{CH}(\text{NH}_2)\text{COOH}$
Serine	$\text{HOCH}_2\text{CH}(\text{NH}_2)\text{COOH}$
Threonine	$\text{CH}_3\text{CH}(\text{OH})\text{CH}(\text{NH}_2)\text{COOH}$
Monoaminodicarboxylic and Amide Derivatives	
Aspartic Acid	$\text{HOOCCH}_2\text{CH}(\text{NH}_2)\text{COOH}$
Asparagine	$\text{NH}_2\text{COCH}_2\text{CH}(\text{NH}_2)\text{COOH}$

Glutamic Acid	$\text{HOOCCH}_2\text{CHOHCHNH}_2\text{COOH}$
Glutamine	$\text{H}_2\text{N COCH}_2\text{CH}_2\text{CH}(\text{NH}_2)\text{COOH}$
Diaminocarboxylic Acids	
Lysine	$\text{HN}=\text{C}(\text{NH}_2)\text{N}(\text{CH}_2)_3\text{CH}(\text{NH}_2)\text{COOH}$
Hydroxylysine	$\text{H}_3\text{N}^+\text{CH}_2\text{CH}(\text{OH})\text{CH}_2\text{CH}_2\text{CH}(\text{NH}_2)\text{COO}^+$
Arginine	$\text{NH}_2\text{CNH}(\text{CH}_2)_3\text{CH}(\text{NH}_2)\text{COOH}$ $\begin{array}{c} \parallel \\ \text{NH} \end{array}$
Sulfur-Containing Amino Acids	
Cysteine	$\text{H}_3\text{N}^+\text{CH}(\text{CH}_2\text{SH})\text{COO}^-$
Cystine	$[\text{SCH}_2\text{CHNH}_2\text{COOH}]_2$
Methionine	$\text{CH}_3\text{SCH}_2\text{CH}_2\text{CH}(\text{N}^+\text{H}_3)\text{COO}^-$
Aromatic Amino Acids	
Phenylalanine	$\text{C}_6\text{H}_5\text{CH}_2\text{CH}(\text{NH}_2)\text{COOH}$
Tyrosine	$\text{OH}(\text{C}_6\text{H}_5)\text{CH}_2\text{CH}(\text{NH}_2)\text{COOH}$
Heterocyclic Amino Acids	
Histidine	$\text{HN}-\text{C}(\text{H})=\text{N}-\text{C}(\text{H})=\text{C}-\overset{\text{H}_2}{\text{C}}-\text{CH}(\text{NH}_2)\text{COOH}$
Proline	$\text{HN}-(\text{CH}_2)_3-\overset{\text{H}}{\text{C}}-\text{COOH}$
Hydroxyproline	$\text{HN}-(\text{CH}_2)_2-\overset{\text{H}(\text{OH})}{\text{C}}-\overset{\text{H}}{\text{C}}-\text{COOH}$
Tryptophan	$\text{C}_6\text{H}_5-\overset{\text{H}}{\text{N}}-\text{C}(\text{H})=\text{C}-\overset{\text{H}_2}{\text{C}}-\text{CHNH}_2\text{COOH}$

Amino acids in proteins and peptides are estimated, after a hydrolysing agent breaks the peptide bonds and they are set free. There are three kinds of hydrolysing methods, which can be used. Each has advantages in particular cases. Since the hydrolytic procedure is of crucial importance, and the hydrolysing agent used effects the amino acid composition, these methods are briefly described in the coming paragraphs.

3. HYDROLYSIS METHODS

3.1. ACID HYDROLYSIS: Dilute H_2SO_4 (5 to 6 N) was used in many of the earlier investigations on protein structure, but extensive losses of amino acids were reported due to their absorption on precipitated BaSO_4 [1]. This method is generally not employed now. The most usually employed acidic reagent is 6N HCl [2]. It has advantage that it can be removed readily from the hydrolysate; the most serious problem is the loss of tryptophan, whereas threonine, serine and tyrosine are partly destroyed [3]. In this method methionine and cystine were either partially destroyed or oxidised to methionine sulphone and cysteic acid [4]. Most of these problems arose from the presence of oxygen in the hydrolysing solution and the presence of the free halogen in the 6N HCl [2]. The difficulty of incomplete hydrolysis has been overcome by increasing the duration of hydrolysis from 24 hours to 72 hours [4]. Tryptophan has been recovered by using 3N p-Toluene Sulphonic acid and a two- percent (2%) protective agent, 3(2-amino ethyl) indole, as hydrolyzing agent in the method developed by Liu and Chang [2]. In the most recent procedure for hydrolysis, a double distilled HCl (6N), free from halogen, is used [4].

3.2. ALKALINE HYDROLYSIS: Alkaline hydrolysis of protein is of limited use. The destruction of arginine, serine, threonine, cysteine and cystine precludes its general application [5]. It is usually applied only in determining amino acids that are labile to acids, in particular tryptophan [6]. Tryptophan is destroyed least when hydrolyses with 4N $\text{Ba}(\text{OH})_2$ is carried out at 110 C° for 50 to 70 hours [6]. The hydrolysates after precipitation of excess of barium, is subjected to chromatographic separation of amino acids.

3.3. ENZYMATIC HYDROLYSIS: To avoid the marked losses of certain amino acids that occur during acid hydrolysis and for the estimation of asparagines and glutamine, enzymatic hydrolysis provides best method [7]. Hill and Schmidt [7] demonstrated that digestion of a protein by papain followed by treatment with the purified protein peptidases and prolidases

gave essentially complete hydrolysis of all peptide bonds and liberated tryptophan, glutamine and asparagines in high yield. Although this is a useful method of hydrolysis, it cannot replace acid hydrolysis because of the operational difficulties involved in the use of enzymes. Nevertheless, it is a valuable supplement to other methods.

For instrument calibration, most laboratories use free amino acids as standards but some laboratories are also subjecting free amino acids to hydrolysis prior to analysis. Some of the laboratories are also reported using hydrolyzed peptides and proteins as standard for instrument calibration. It was noted that use of automated derivatization and hydrolysis has increased [8]. Performic (peroxomethanoic acid) oxidation is most reliable for the analytical determination of cystine, cysteine, and methionine when tryptophan is absent [8]. In the estimation of tryptophan an average error of as high as 85.1 % was reported by many laboratories [8]. Some laboratories which reported low percentage of tryptophan error used HCl hydrolysis in the presence of dodecanethiol, suggesting this to be a superior technique for tryptophan [8].

4. ION EXCHANGE RESINS USED FOR ANALYSIS

Amino acids in a protein hydrolysate can conveniently be separated for qualitative and quantitative analyses by paper or thin layer chromatography, electrophoresis, and with great convenience and accuracy by automated ion exchange chromatography.

Two general classes of immobile ion exchangers are most frequently used by biochemists [8],

- (a) Synthetic resin backbone ion exchangers, and
- (b) Polysaccharide backbone ion exchangers.

In this review we would like to focus on the ion exchange resins having synthetic backbone only. They are porous and elastic particles, containing synthetic resin backbone, usually of polystyrene type, formed by the

copolymerization of styrene and divinyl benzene (Fig. 2). Desired functional groups, such as strongly acidic ($-\text{SO}_3\text{H}$), strongly basic ($-\text{NR}_3^+$), weakly acidic ($-\text{COOH}$) and weakly basic ($-\text{NH}_3^+$) can be introduced by the replacement of styrene with corresponding substituted styrene analog. Table 2 gives some of the commonly used polystyrene type ion exchange resins.

5. DEVELOPMENT IN THE METHOD OF AMINO ACID ANALYSIS USING ION EXCHANGE RESINS

Griessbach [9] was one of the first to separate amino acids with the aid of ion exchange resins. Freedenberg [10] and also Block [11] described methods for the separation of amino acids into groups and also for their separation from non-electrolytes, with ion exchangers. Since 1945, many papers have appeared by various workers on the chromatographic separation of amino acids with ion exchange resins.

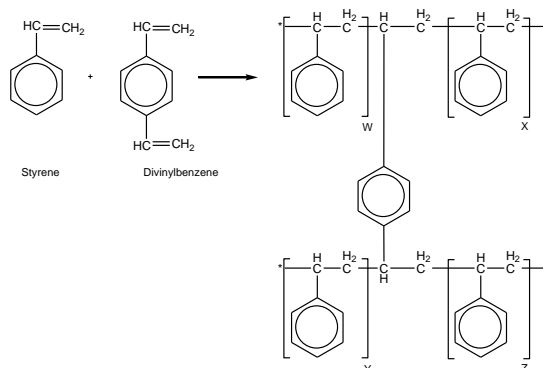

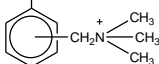
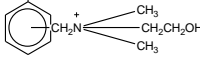
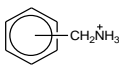
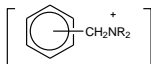
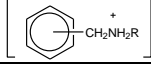


Fig. 2: Copolymerization of styrene and divinyl benzene makes polystyrene resins.

Table 2: Polystyrene type ion exchangers and their characteristics

Name	Class	Functional group
DOWEX 50	Cation exchanger (strong)	
IRC 150	Cation exchanger (weak)	
DOWEX 1	Anion exchanger (strong)	
DOWEX 2	Anion exchanger (strong)	
IR 45	Anion exchanger (weak)	
DOWEX 3	Anion exchanger (weak)	

Adsorption and separation of the amino acids on the ion exchanger depends upon their dissociation constants. Anion exchangers in acid form will adsorb all amino acids and any non-electrolytes such as sugar will be separated from them [12]. By using these resins in the neutralized form i.e. Na^+ or NH_4^+ form, neutral amino acids can be selectively adsorbed and dicarboxylic acids and histamine will not be adsorbed [12]. Weakly acidic resins are more suitable for separation of all types of amino acids [12]. Various ion exchangers have been used by Tiselius [13] to separate all amino acids. Four columns were used in the work. The three columns were: i) charcoal, ii) wolfatit C (a carboxylic acid resin), iii) wolfatit KS (a sulphonic acid resin) and iv) Amberlite IR 4 (Cl^-). The first column adsorbed the aromatic amino acids and let the others pass. The second removed the basic amino acids (arginine, lysine, histidine), and third adsorbed the remaining neutral and acidic amino acids. The eluate from the third column was passed through the fourth column containing Amberlite IR 4 (Cl^-), where neutral acids and those containing two carboxylic groups were separated by elution with water and 1M HCl, respectively. This whole exercise took two days.

Partridge and Brimbley [14] have devised method for separation of amino acids based on displacement chromatography. Like above, aromatic amino acids were adsorbed on a column of activated charcoal instead on a resin as they might react with it. A clear solution, free from suspended matter was passed through Zeo-Karb 215, to adsorb basic amino acids, and then passed through an anion exchanger Dowex 2 to adsorb the remaining amino acids (neutral and acid). Particle size of resins used is usually 60-80 mesh for smaller columns and 100-120 mesh for larger columns. Details on crushing down the resins to the required particle size by the use of a ball mill are available in literature [14]. In order to achieve greater exchange capacity multiple columns can be arranged in series. The separation and the order of elution achieved by Partridge and Brimbley [14] is given in Table 3. The acids shown in square brackets eluted together because of closer pK values. They may be separated by passing through an anion exchanger of opposite charges. The authors used this method to separate amino acids from 64 g of egg albumen by use of a column packed with Zeo-Karb 250 (SO_3^-) and 0.15 M ammonium hydroxide used as an eluant. The fractions were collected and tested with paper chromatography and seven groups of amino acids, including i) aspartic acid, ii) glutamic acid, serine and threonine, iii) glycine and alanine, iv) valine and proline, v) leucine, isoleucine, methionine and cystine, vi) histidine, glucosamine, and vii) lysine were detected. Some of the bands were further separated by rechromatography on Zeo-Karb 215 and chromatography on Dowex 2 (an anion exchanger). Partridge [15], after his wide separation experience, recommended polystyrene sulphonic acid resins for this purpose as they are faster than the phenolic resins and give better separations. It was discovered that 5% cross-linked resins were better than those having higher cross linkage because of swelling problems. Moore and Stein [16] demonstrated that a mixture of 18 amino acids could be resolved completely on a Dowex 50-X8 using hydrochloric acid as eluant. Moore and Stein [17] achieved separation of 32 components of a synthetic mixture of amino acids using citrate-bicarbonate buffers of progressively increasing pH from 3.4 to 11.0. Small amounts of detergent and thiodiglycol were

added to the solution of acids to increase the rate of flow and reduce losses due to the oxidation of methionine, respectively. Further modifications in the procedure were made by using Dowex 50 and gradient elution. By this modified procedure a synthetic mixture of fifty components was resolved on 150-cm column.

Table 3: Order of elution of amino acids [14]

Polystyrene-SO ₃ H column			Dowex 2 column		
Aspartic acid	pK ₁	1.88	Lysine	pK ₃	10.50
Hydroxy proline	pK ₁	1.92	Proline	pK ₂	10.60
Threonine	-	-	β-Alanine	"	10.19
Serine	pK ₁	2.21	Alanine	"	9.69
Glutamic acid	"	2.19	Valine	"	9.62
Proline	"	1.99	Leucine	"	[9.60]
Glycine	"	2.23	Gycine	"	[9.60]
Alanine	"	[2.34]	Carnosine	"	9.51
Valine	"	[2.32]	Threonine	--	--
Methionine	"	2.28	Serine	"	9.15
Leucine	"	2.36	Histidine	pK ₃	9.17
Cystine	"	2.26	Methionine	pK ₂	9.21
Creatine	"	Ca 3.0	Methyl histidine	pK ₃	8.82
Phenyl alanine	"	1.83	Cystine	pK ₂	7.82
β-Alanine	"	3.60	Tyrosine	pK ₂	9.11
Trimethyl amino oxide	pK	Ca 4.55	Acetic acid	pK ₂	4.75
Creatinine	pK	Ca 4.8	Glutamic acid	pK ₂	4.25
Histidine	pK ₂	6.0	Aspartic acid	pK ₂	3.65
Methyl histidine	"	6.48			
Carnosine	"	6.83			
Anserine	"	7.04			
Hydroxy lysine	--	--			
Lysine	pK ₂	8.98			
Ammonia	pK	9.27			
Arginine	pK ₂	9.04			
Methyl amine	pK ₁	10.64			

In the latest procedure the bead form of Dowex resins have been abandoned in favour of "micro powder" from 8% cross-linked resin Amberlite IR-120. The resolution and sensitivity improved significantly, but a poor flow rate was observed. Two columns filled with Amberlite IR-120 were employed, one for the separation of neutral and acidic amino acids (150 cm) and second for the separation of basic amino acids (15 cm). Moore et al. [18] were able to perform a complete amino acid analysis in 48 hours using a manual method of collecting fractions and then developing

the colour with Ninhydrin.

6. AUTOMATION IN AMINO ACID ANALYSIS

Automation was achieved by slowly pumping the buffer carrying the amino acids down the column, as it emerged through the column it was met by a stream of ninhydrin reagent from a tube. The mixture was heated in a boiling water bath, where reaction between the amino acids and ninhydrin took place to form a blue colour. The optical density was measured quantitatively at 570 nm (440 nm for proline) by colorimeters. The output of the detector is fed to a chart recorder. Each amino acid is identified by its time of elution and its quantity determined from the area of the peak on the chart.

Piez and Morris [19] attempted to improve the methods using column and gradient to obtain complete analyses in single run, but it took longer time. Hamilton [20] used a single column with discontinuities. The sensitivity was increased 100 times compared to the earlier methods. Simmonds and Rowlands [21] and Dus et al. [22] achieved success in analyzing as many as 6-8 samples simultaneously, using automatic techniques. Methyl cellosolve was added to 4N sodium acetate to increase its solubility. Stannous chloride ($\text{SnCl}_2 \cdot 2\text{H}_2\text{O}$) was added to avoid side reactions and increase the reproducibility of the colour development. Fig. 3 represents a typical chromatogram obtained from an automatic amino acid analyzer, Moore and Stein [23] procedure. The peaks on the chromatogram represent individual amino acids. The order of their coming out of the column is from left to right.

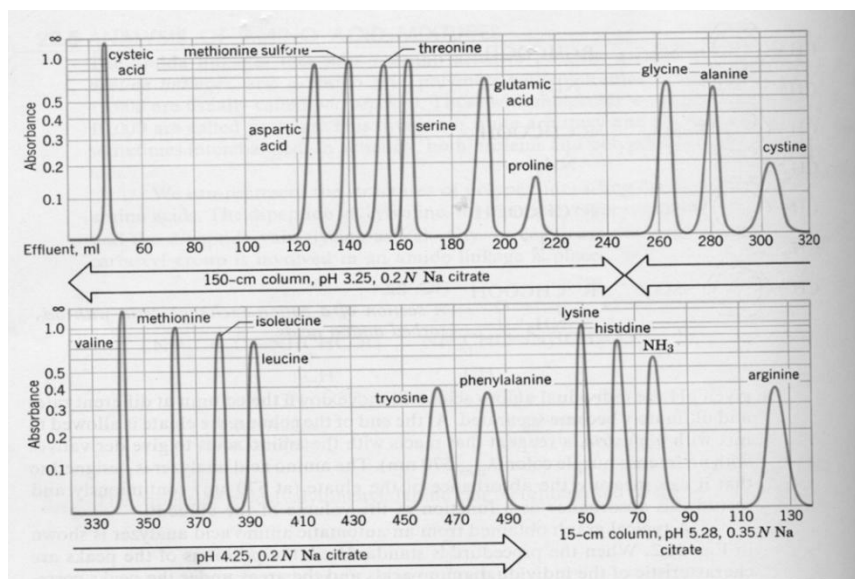


Fig. 3: A typical protein fractionation into amino acids using cation exchange resin chromatography [23]

7. REACTION OF NINHYDRIN WITH AMINO ACIDS

The colour reaction between amino acids and triketohydrate hydrate (ninhydrin) has been studied extensively. Several authors [24-28] have described the use of ninhydrin in amino acid estimation. Colored compounds are formed not only with amino acids but also with proteins and peptides, and other compounds with free amino groups. Ninhydrin reacts to decarboxylate the amino acids, and yield an intensively colored purple blue product (I) having absorption maximum at 570nm, carbon dioxide, water and aldehydes. The reagent also reacts with imino acids e.g. proline to give a yellow colored product (II) having absorption maximum at 440 nm. Amino acids react with fluorescamine, and ortho-phthalaldehyde and mercaptoethanol to yield products that provide more sensitive means of analyzing amino acid mixtures. The reaction of ninhydrin with amino acid is very sensitive and is represented in Fig. 4.

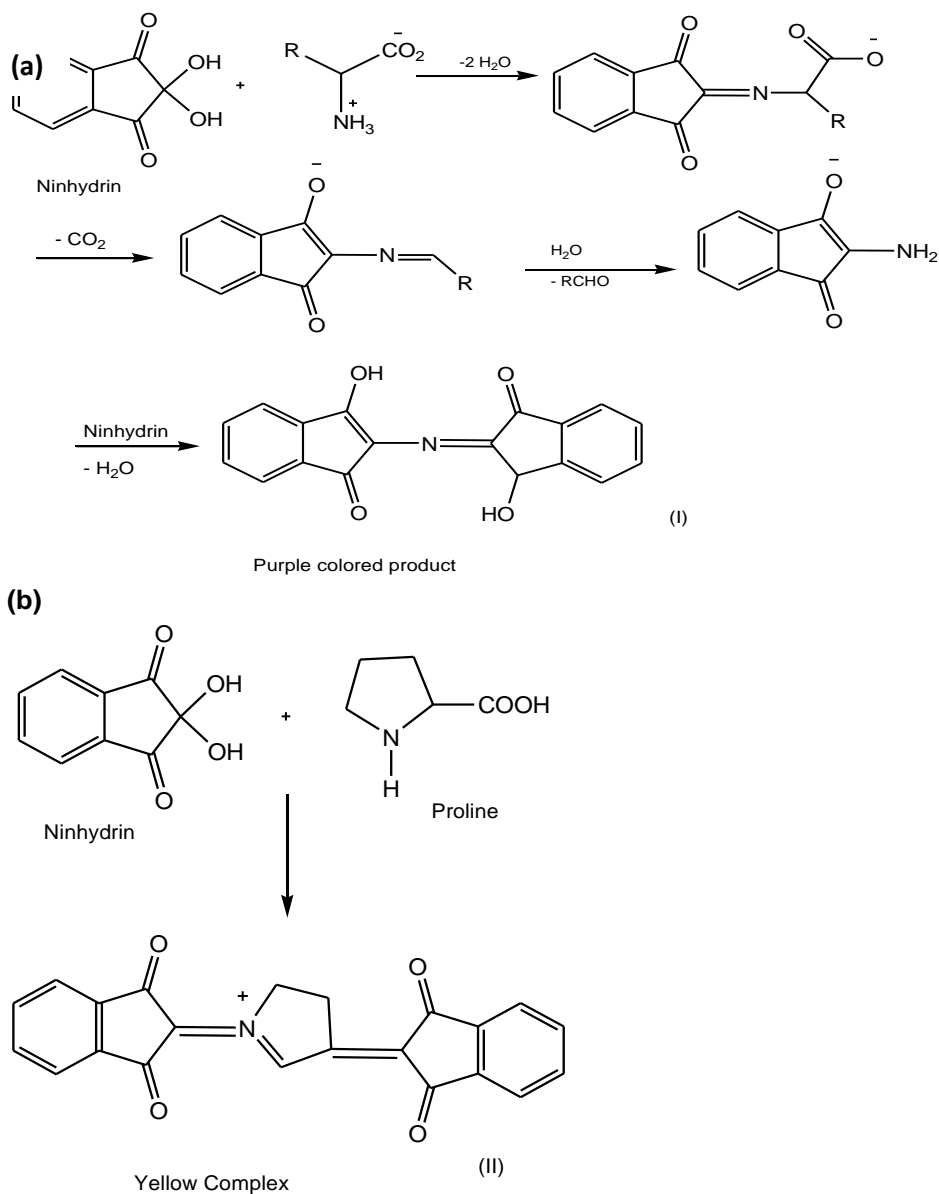


Fig. 4: Reactions of ninhydrin with (a) amino acid and (b) imino acid (proline)

Williams [29] has summarized thirty years of collaborative trials to assess the reliability of the amino acid analysis techniques. Association of Biomolecular Resource Facilities (ABRF) made a series of trials, others [30-33] provided information on various aspects of amino acid analysis using ion exchange chromatography. ABRF studies examined recovery, accuracy and precision of amino acid analysis using synthetic peptides, purified

protein or protein hydrolysates. Amino acid Analysis Research Committee reported [34] that an average error among participants has been 10-12%. Errors due to hydrolysis and chromatographic analysis in amino acid analysis have been separately discussed and method for analysis of cystine/cysteine and tryptophan were tested [31, 35]. Pre-column treatment is considered to be more sensitive as compared with post-column approach. A number of pre-column derivatization options have been discussed by Furst et al. [36]. Other advantages of the pre-column derivatization include sensitivity, U.V detection as opposed to fluorescence and stability. Phenylisothiocyanate (PITC) is by far the most common reagent studied for pre-column treatment [37]. Free amino acids and their derivatives in tse tse fly (*Glossina palpalis*) were separated using ion exchange chromatography [38]. Rapid automated ion exchange analysis of plasma and phenylalanine was carried out by Tarbit et al. [39]. Twenty amino acids, including aminoethylcystein, were separated from acid hydrolysates of insulin and Lysozyme on single column by Gannor et al. [40]. Basic amino acids were isolated and concentrated by ion exchange chromatography from complex biological samples prior to high performance liquid chromatography [41]. Duran et al. [42] used amino acid analyzer for the study of amino acid disorders. Amino acids were analyzed in biological fluids by automated ion exchange chromatography by Bouchar et al. [43]. Ion exchange chromatography was used to purify proteins from white perch (*Morone americana*) by Hiramatsu et al. [44]. Analysis of plasma amino acids in amyotrophic lateral sclerosis patients was performed on ion exchange chromatography using automatic amino acid analyzer [45]. Ion exchange resin column also has been used [46] to separate carbohydrates from amino acids.

Free amino acids in wines were determined using ion exchange chromatography by Cosmos and Sarkardi [47]. HPLC method was found to be comparable with ion exchange chromatography [48, 49]. Determination of tryptophan in proteins and feed stuff has also been carried out by ion exchange chromatography [50].

Mustafa et al. [51] used gas chromatography after ion exchange chromatography to analyze amino acids. Terrab et al. [52] used reverse phase HPLC with pre-column PITC derivatisation to analyses free amino acids in nectar of *Silene colorata* Poiret (Caryophyllaceae).

Cereal proteins have been hydrolyzed and analysed. The values obtained for α_1 -Gliadin, α_2 -Gliadin, β_1 -Gliadin and β_1^* -Gliadin [53] are presented in Table 4.

Table 4: Amino acids analysis of some Gliadins (cereal proteins) using ion exchange resins [53]

Amino acid	Moles per 10 ⁵ g of recovered anhydro-amino acids			
	α_1 -Gliadin	α_2 -Gliadin	β_1 -Gliadin	B ₂ - Gliadin
Aspartic acid	26.7(8)	18.5(4)	21.4(6)	14.4(4)
Threonine	71.9(23)	32.0(7)	25.8(7)	6.5(2)
Serine	86.28(27)	83.0(18)	74.7(21)	14.6(4)
Glutamic acid	232.6(73)	332.6(73)	297.4(82)	358.6(108)
Proline	110.9(351)	173.6(38)	167.2(46)	188.8(57)
Glycine	44.5(14)	21.4(5)	19.7(6)	17.4(5)
Alanine	45.3(14)	24.8(5)	24.7(7)	20.6(6)
Cystine	58.2(19)	26.2(6)	21.9(6)	7.0(2)
Valine	41.3(13)	22.4(5)	30.9(9)	34.7(11)
Methionine	29.1(9)	10.2(0)	10.4(3)	13.9(4)
iso-Leucine	30.5(10)	18.2(4)	28.7(8)	38.8(12)
Leucine	50.0(16)	51.2(11)	62.0(17)	60.1(18)
Tyrosine	22.0(7)	18.2(4)	19.2(5)	19.1(6)
Phenylalanine	22.0(7)	42.0(9)	37.3(10)	26.5(8)
Lysine	3.2 (1)	4.5(1)	3.6(1)	3.3(1)
Histidine	11.11 (4)	10.6(20)	16.8(5)	15.7(5)
Arginine	24.8 (8)	13.5(3)	16.5(5)	14.1(4)

*Cystine determined as carboxymethylcystine

figures are nearest integers residues obtained by taking lysine as unity.

8. CONCLUSIONS

In the light of the authors experience about amino acid analysis, using various techniques, it can be stated that although there are recently developed methods of amino acid analyses, such as gas chromatography,

which are faster and less expensive, ion exchange method of amino acid analysis is the best despite its being expensive, and will continue to be used for this purpose for years to come because of its reproducibility, recently achieved better speed, and complete automation.

REFERENCES

1. T. E. Hugli and S. Moore, *J. Biol. Chem.*, 247 (1972) 2828.
2. T. Y. Lu and Y. Y. Chang, *J. Biol. Chem.*, 246 (1971) 2843.
3. M. G. Davies and A. J. Thomas, *J. Sci. Food Agri.*, 24 (1973) 1525.
4. G. E. Tarr, *Methods of Protein Microcharacterization* (Shivley J.E. Ed). Humana Press, Clifton NJ., (1986).
5. S. Moore and W. H. Stein, *Methods in Enzymology*, Volume 6, Academic Press, New York, (1963).
6. E. A. Noltman, T. A. Mahowald and S. A. Kuby, *J. Biol. Chem.*, 237 (1962) 1146.
7. R. L. Hill and W. R. Schmidt, *J. Biol. Chem.*, 237 (1962) 389.
8. K. A. West and J. W. Crabb, *Techniques in Protein Chemistry III*, (Angelletti R.H.ed) Academic Press, New York., (1992).
9. R. Griessbach, *Angew. Chem.*, 52 (1939) 215.
10. K. Freedenberg, *Organische Chemie*, Heidelberg Quelle U. Meyer, (1948).
11. R. J. Block, *Pro. Sec. Exp. Biol. Med.*, 72 (1949) 337.
12. S. Nazaki, *Separation Method of Amino Acids*, US Patent 53006539 (1994).
13. A. Tiselius, *Experintia.*, 17 (1961) 433.
14. S. M. Partridge and R. C. Brimley. *Biochem. J.*, 51 (1952) 628.
15. S. M. Partridge, *Biochem. J.*, 44 (1949) 521.
16. B. Moore and W. H. Stein, *Quant. Biol.*, 14 (1950) 179.
17. S. Moore and W. H. Stein. *J. Biol. Chem.*, 192 (1951) 663.
18. S. M. Moore, D. H. Spackman and W. H. Stein, *Anal. Chem.*, 30 (1958) 1185.
19. K. A. Piez and L. A. Morris, *Anal. Biochem.*, 1 (1960) 187.
20. P. B. Hamilton. *Anal. Chem.*, 35 (1963) 2055.

21. D. H. Simmonds and R. J. Rowland, *Anal. Biochem.*, 32 (1960) 259.
22. K. A. Dus, M. Dekker and R. M. Smith, *Anal. Biochem.*, 11 (1965) 312.
23. S. Moore and W. H. Stein, *J. Biol. Chem.*, 176 (1948) 367.
24. S. Moore and W. H. Stein, *Methods in Enzymology*, Vol. 6, Academic Press, New York, (1963).
25. W. Troll and R. K. Cannon., *J. Biol. Chem.*, 200 (1953) 803.
26. E. W. Yemm, E. C. Cocking and R. E. Recketts, *Analyst*, 80 (1955) 209.
27. J. Heilmann, J. Barolier and E. Watzke, *Physiol. Chem.*, 309 (1957) 219.
28. C. S. Hanes, A. T. Matheson and E. Tigane, *Can. J. Biochem. Physiol.*, 39 (1961) 417.
29. A. P. Williams, *Amino acid Analysis*, Ellis Harwood Ltd. New York., (1981).
30. R. L. Niece, J. Elliot, K. L. Stone, W. J. McMurray, A. Fowler, D. Atherton, R. Kutney and A. Smith, *Techniques in Proteins Chemistry*, Academic Press, San Diego, (1989).
31. J. W. Crabb, A. J. Smith and, R. Kutny., *Current Research in Protein Chemistry*, Academic Press, San Diego, (1990).
32. L. H. Ericsson, D. Atherton, R. Kutny, A. J. Smith and J. W. Crabb, *Method of Protein Sequence Analysis*. (H. Jornvall and J.O. Hogg Eds.) Birchauser, Verlag, Basel, (1991).
33. G. E. Tarr, R. J., Paxton, Y. C. E. Pan, L. H. Ericsson and J. W. Crabb, *Techniques in Protein Chemistry II*, Academic Press, San Diego, (1991).
34. K. U. Yuksel, T. T. Andersen, I. Apostol, J. W. Fox, J. W. Crabb and D. J. Strydom, *Techniques in Protein Chemistry VI*, (Crabb, J. W. Ed.) Academic Press, San Diego, (1994).
35. D. J. Strydom, T. T. Anderson, I. Apostol, J. W. Fox, R. J. Paxton, and J. W. Crabb, *Techniques in Protein Chemistry IV*. Academic Press, San Diego, (1993).
36. P. Furst, L. Pullack, F. A. Gracer, H. Goldel and P. Stehle, *J. Chromat.*, A 499 (1990) 557.

37. M. I. Perl, *J. Chromat.*, A 661 (1969) 43.
38. R. A. Balogun, C. Hanimann and P. S. Chen. *Cell. Mol. Life Sci.*, 25 (1969) 93.
39. I. F. Tarbit, J. P. Richardson and G. Dale, *J. Chromat. B and Biomedical Sciences Applications*, 18 (1980) 337.
40. S. Gannor, Y. Hamno, J. Kobaryashi and T. Masaki, *J. Chromat.*, A 332 (1985) 278.
41. S. G. Rebecca, G. G. Guadelupe, H. Leo and V. B. Craig, *Anal. Biochem.*, 197 (1991) 86.
42. M. Duran, L. Dorland, P. K. Bree and R. Berges, *Eur. J. Pediat.*, 153 (1994) S33.
43. J. L. Bouchar, C. Charet, C. Coundray-lucase, J. Gibudeau and L. Cynober, *Clin. Chem.*, 43 (1997) 1421.
44. N. Hiramatsu, T. Matsubara, A. Hara, M. Danato, K. Hiramatsu, N. D. Denslow and C. N. Sullivan, *Fish Physiol. and Biochem.*, 26 (2002) 355.
45. J. Illzecka, Z. Stelmasiak, J. Solski, S. Wawrzyki and M. Szentnar, *Amino acids.*, 25 (2003) 69.
46. Y. Ding, H. Yu and S. Mou, *J. Chrom.*, 997 (2003) 155.
47. E. Cosmos and S. L. Sarkardi, *Chromatographia*, 56 (2002) S185.
48. L. S. Elisabeth, L. R. William and P. Marzia, *Clin. Chim. Act.*, 354 (2005) 83.
49. D. Fekkes, A. Voskuilen-Kooyman, R. Jankie and J. Huijmans, *J. Chrom. B: Biomedical Sciences and Applications*, 744 (2000) 83.
50. G. Ravindran and B. L. Bryden, *Food Chem.*, 89 (2005) 309.
51. A. Mustafa, A. Per, R. Andersson and A. Kamal-Eldin, *Food Chem.* 105 (2007) 317.
52. A. Terrab, J. L. García-Castaño, J. M. Romero, R. Berjano, C. de Vega and S. Talavera, *Botan. J. Lin. Soc.*, 155 (2007) 49.
53. A. K. Saeed, *Studies on Separation and Structure of Gliadin Proteins*, Ph.D. Dissertation (1976), University of London, London, UK.

JOURNAL OF NATURAL SCIENCES AND MATHEMATICS

INFORMATION FOR AUTHORS

1. TYPES OF PAPERS ACCEPTED

The Journal aims at publishing original research papers and the review papers from distinguished scientists on Mathematics, Physics, Chemistry and Computer Science.

2. SUBMISSION OF MANUSCRIPTS

Manuscripts should be submitted in duplicate to the Section Editor concerned. All papers are refereed. The decision of the Editorial Board regarding the acceptance and publication of the paper will be final.

3. PREPARATION OF MANUSCRIPT

3.1 Language and Style

All submissions should be in English, typed in double spacing on one side of the paper only with a left hand margin of at least 4 cm. Mathematical expressions must be carefully printed. Computer composed manuscript on C.D. in Microsoft Word is required for speedy publication.

3.2 Abstract

This should comprise a brief and factual summary of contents and should be suitable for direct use by abstracting journals. This will seldom require more than 200 words.

3.3 Section/Sub-Section Headings

Papers should be divided into sections / sub-sections and numbered as exemplified in the headings of this INFORMATION FOR AUTHORS.

3.4 References

References should be numbered consecutively in the text, e.g. "According to a recent theory [6]...it is well established [7]" and collected at the end of the paper in following style:

6. I. M. Ghauri and P. Feltham, J. Nat. Sci. Math., 26 (1986) 63.

7. W. Greiner and J. Maruhn, Nuclear Models, Springer-Verlag, Berlin, (1996).

3.5 Illustrations

Line diagrams must be drawn in black ink on white paper; original and two copies are required. Photographs or half-tone reproduction should be in the form of highly glazed prints. A separate list of captions for illustrations should be provided.

4. PROOFS

Only one set of proof is sent to the authors for correction.

FUNDAMENTAL GROUP OF THE DYNAMICAL GRAPH

M. EL-GHOUL AND *M. A. EL-FATTAH

Department of Mathematics, Faculty of Science, Tanta University, Tanta, Egypt,
*Department of Mathematics, Faculty of Science, Minoufiya University, Egypt

(Received: January 07, 2008)

ABSTRACT: In this paper we will discuss the dynamical graph and its fundamental group. Also we will study the folding of the dynamical graph and the change of the fundamental group under the folding. The variation of the fundamental group under the variation of time will be discussed. We will study the fundamental group of the simplex and simplicial complex.

Keywords: Graph, dynamical system, fundamental group. 2000
Mathematics Subject classification 51H10,57N20

1. INTRODUCTION

A dynamical system is a concept in mathematics where a fixed rule describes the time dependence of a point in a geometrical space. The mathematical models used to describe the swinging of a clock pendulum, the flow of water in pipe or the number of fish each spring in a lake are examples of dynamical system.

A dynamical system has a state determined by a collection of real numbers. Small changes in the state of the system correspond to small changes in the numbers. The numbers are also the coordinates of a geometrical space- manifold. The evolution rule of the dynamical system is a fixed rule that describes what future states follow from the current state. The rule is deterministic for a given time interval only one future state follows from the current state.

The concept of dynamical system has its origins in Newtonian mechanics. There, as in other natural sciences and engineering disciplines, the evolution rule of dynamical systems is given implicitly by a relation that

gives the state of the system only a short time into the future.

The study of dynamical system has led to the discovery of certain laws of nature which we apply to the current state of a system to predict a future state [1-6]. The different types of folding are discussed in [7,8], and the uncertain folding of manifolds is defined in [9]. Some types of conditional folding and fractal folding are discussed in [10].

2. DEFINITIONS AND BACKGROUND

(1) A dynamical system in the space X is a function $q = f(p, t)$ which assigns to each point p of the space X and to each real number t ($-\infty < t < +\infty$) a definite point $q \in X$ and possesses the following three properties:

(i) Initial condition: $f(p, 0) = p$ for any point $p \in X$.

(ii) Property of continuity in both arguments simultaneously:

$$\lim_{\substack{p \rightarrow p_0 \\ t \rightarrow t_0}} f(p, t) = f(p_0, t_0).$$

(iii) Group property: $f(f(p, t_1), t_2) = f(p, t_1 + t_2)$ [11].

(2) A graph G consists of a non-empty set of elements, called vertices, and a list of unordered pairs of these elements, called edges. The set of vertices of the graph G is called the vertex-set of G , denoted by $V(G)$, and the list of edges is called the edge-list of G , denoted by $E(G)$. If u and v are vertices of G , then an edge e of the form $\{u, v\}$ or $\{v, u\}$ is said to join u and v . the vertices u and v are called the end vertices or ends of the edge e . Each edge is said to join its ends, and e is incident with each one of its ends. Also the vertices u and v are then incident with e and u, v are said to be adjacent. Two or more edges joining the same pair of vertices are called multiple edges, and an edge joining a vertex to itself is called a loop. A graph with no loops or multiple edges is called a simple graph. A graph

is called finite if both $V(G)$ and $E(G)$ are finite. A graph that is not finite is called infinite. A graph is trivial if its vertex set is a singleton and it contains no edges [12].

(3) The fundamental group: Let x be any point of X ; the set of all loops based at x , is a group This group is called the fundamental group of X at the base point x , and denoted by $\pi(X, x)$ [13].

(4) Consider C^∞ Riemannian manifolds M and N , of dimensions m and n respectively such that $m \leq n$. A map $f : M \rightarrow N$ is said to be an isometric folding of M into N iff for every piecewise geodesic path $\gamma : J \rightarrow M$, the induced path $f \circ \gamma : J \rightarrow N$ is piecewise geodesic and of the same length as γ [14].

(5) Let M and N be two Riemannian manifolds of the same dimensions, a map $g : M \rightarrow N$ is said to be an *unfolding* of M into N if, for every piecewise geodesic path $\gamma : I \rightarrow M$ ($I = [0,1] \subset \mathbb{R}$), the induced path $g \circ \gamma : I \rightarrow N$ is piecewise geodesic but with length greater than that of γ [15].

(6) The (closed) simplex with vertices v^0, v^1, \dots, v^n is the set of points a -dependent on v^0, v^1, \dots, v^n and with every barycentric coordinate ≥ 0 , where v^0, v^1, \dots, v^n are a -independent [16].

(7) A simplicial complex is a finite set K of simplexes in \mathbb{R}^n with the following two properties:

(i) if $s \in K$ and $t \subset s$ then $t \in K$,

(ii) intersection condition : if $s \in K$ and $t \in K$ then $s \cap t$ is either empty or else a face both of s and of t . The dimension of K is the largest dimension of any simplex in K [16].

(8) A subset A of a topological space X is called a retract of X if there exists a continuous map $r : X \longrightarrow A$ (called a retraction) such that $r(a) = a$ for any $a \in A$ [13].

3. THE MAIN RESULTS

Proposition 1: The fundamental group of the trivial dynamical graph is isomorphic to zero.

Proof: The trivial graph is (v_i, \emptyset) , since the dynamical graph will be either the same graph or will change into graph with edges, in the two cases the fundamental group is isomorphic to zero. See Fig. 1.

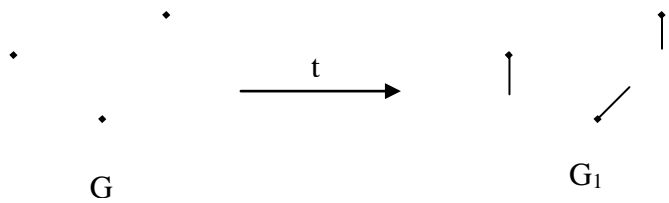
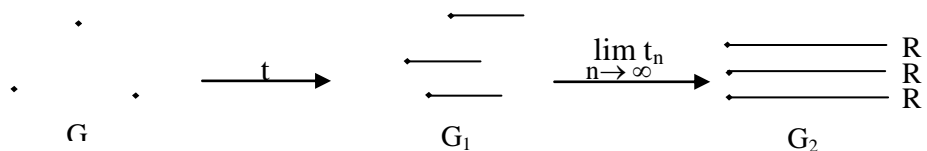


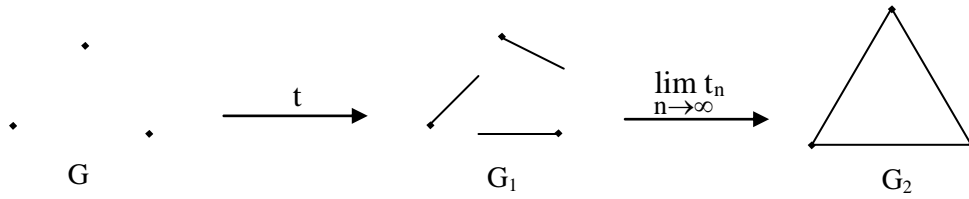
Fig. 1

Proposition 2: The fundamental group of the singleton dynamical graph is not necessary isomorphic to zero.

Proof: Let (v_i, \emptyset) be the singleton dynamical graph if the variation of the time changes the dimension of the graph to one, i.e., the vertices grow to be an edges and there are no loops, multiple edges or closed paths, then the fundamental group is still isomorphic to zero. But when the variation of time make the vertices grow to touch each other, in this case the dimension is one and there are loops, multiple edges and closed paths, here, the fundamental group converts to be isomorphic to one. See Fig. 2.



(a)



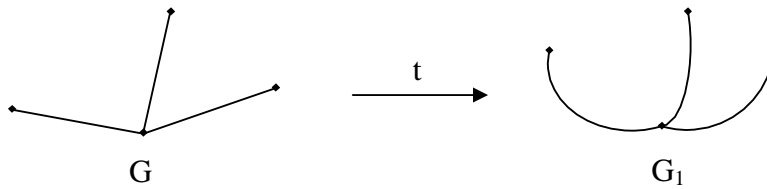
(b)

Fig. 2

In Fig. 2 (a) the limit of variation of time has no effect on $\pi(G)$ which isomorphic to 0. But in (b) we have $\pi(G) = \pi(G_1) \cong 0$, and $\pi(G_2) \cong \mathbb{Z}$, where $G = \lim_{n \rightarrow \infty} t_n(G)$.

Proposition 3: The fundamental group of the dynamical graph of dimension one is not necessary change by the time.

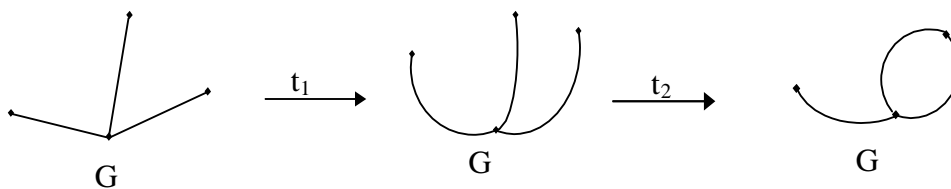
Proof: Since the fundamental group of the graph if it is a simple graph and has not any closed paths is isomorphic to zero. So, if the variation of time does not make any loops, multiple edges or closed paths then the fundamental group is unchanged (isomorphic to zero), but the fundamental group of this dynamical graph may be changed under variation of time, as follows in Fig.3 (a) and (b).



(a)

We have $\pi(G) = \pi(G_1) \cong 0$.

The effect of the dynamical change under the time t is equivalent to the folding, $f : G \longrightarrow G_1$.



(b)

Fig. 3

In this case we have $\pi(G) = \pi(G_1) \cong 0$, but $\pi(G_2) \cong Z$. And the limit of this dynamical change is G_n , it may by looks like



, then $\pi(G_{n1}) \cong Z \oplus Z$ and $\pi(G_{n2}) \cong Z$. Or the dynamical graph changed in different way then also its limit and its fundamental group changed.

Example 1: The folding of the dynamical graph G_1 and the limit of foldings of G_1 into itself as follows.

$f_1: G_1 \longrightarrow G_1, f_1(G_1) = G_2$, such that, $f_1(v_0) = v_0, f_1(v_1) = v_1, f_1(v_2) = v_2$ and $f_1(v_3) = v_0$.

$f_2: G_2 \longrightarrow G_2, f_2(G_2) = G_3$ such that, $f_2(v_0) = v_0, f_2(v_1) = v_1$ and $f_2(v_2) = v_0$, (see Fig. 4)

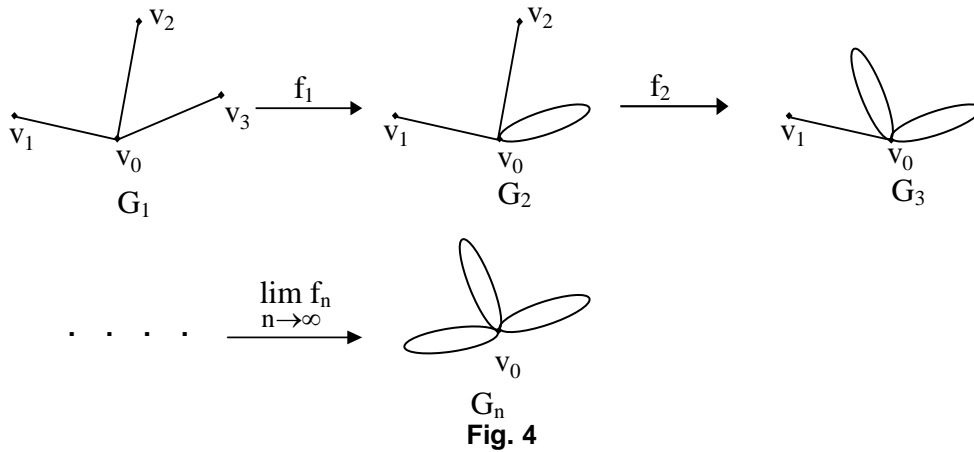


Fig. 4

In this example we have, $\pi(G_1) \cong 0, \pi(G_2) \cong Z, \pi(G_3) \cong Z \oplus Z$ and $\pi(G_4) \cong Z \oplus Z \oplus Z$.

The effect of the dynamical change under the time t is equivalent to this type of folding.

Example 2: $f: G_1 \longrightarrow G_1, f(G_1) = G_2$, such that, $f(v_1) = v_1, f(v_2) = v_2, f(v_3) = v_3$ and $f(v_4) = v_2$ (see Fig. 5)

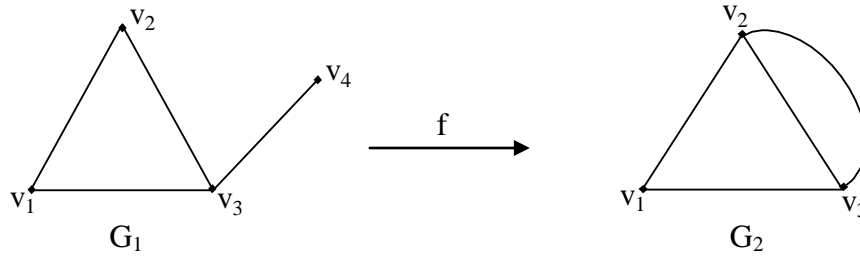
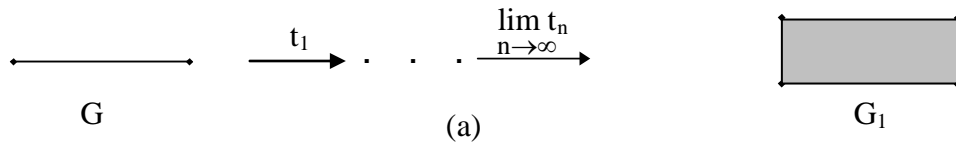


Fig. 5

then $\pi(G_1) = \pi(G_2) \cong \mathbb{Z}$.

Example 3: The dynamical graph G , which consists of two vertices and one edge, changes under variation of time to be as simplicial complex with four vertices. Fig. 6.



$\pi(G) = \pi(G_1) \cong 0$,

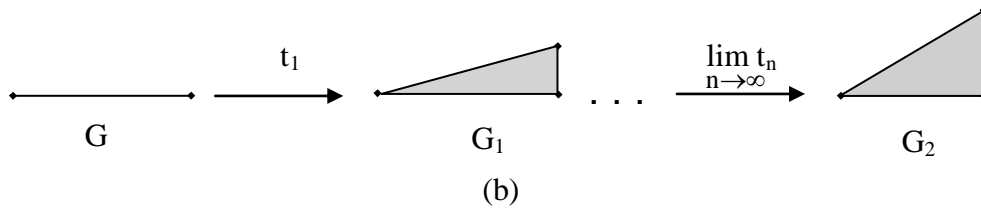
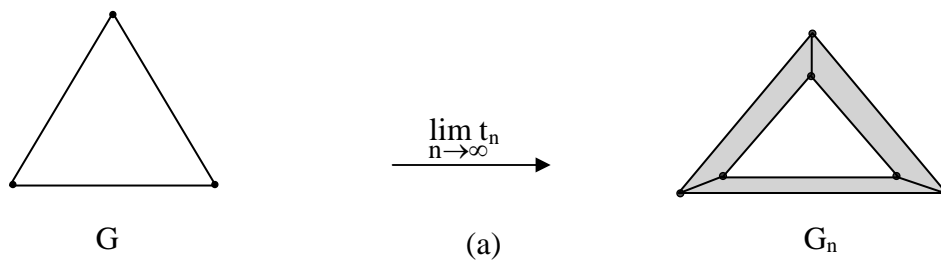


Fig. 6

$\pi(G) = \pi(G_1) = \pi(G_2) \cong 0$

Example 4: The dynamical graph G which grows under the limit of variation of time t to be G_n and G_1 which are simplicial complexes, as shown in Fig. 7 (a) and (b).



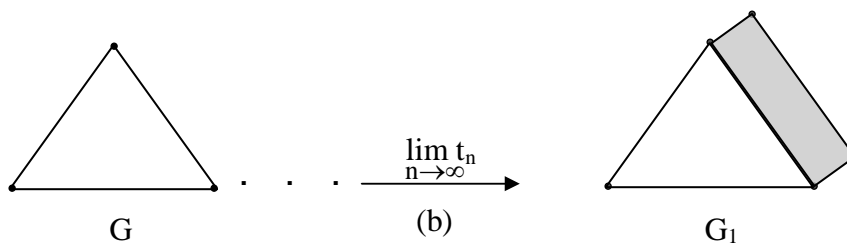
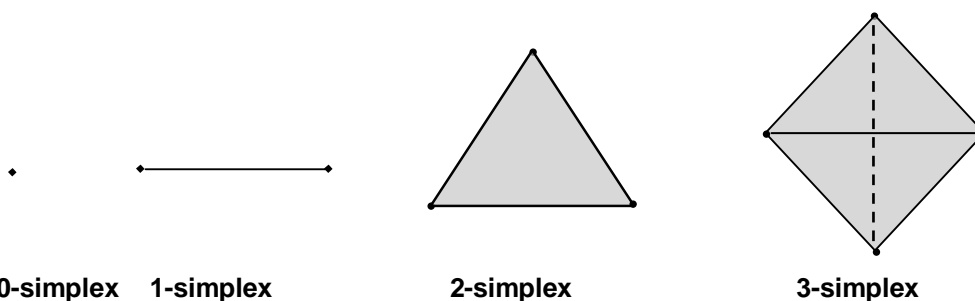


Fig. 7

In this example the limit of variation of time t has no effect on $\pi(G)$. Thus in (a) we have $\pi(G) = \pi(G_n) \cong \mathbb{Z}$, and in (b) $\pi(G) = \pi(G_1) \cong \mathbb{Z}$.

Also, the retraction with removing a point $r_1: G_n \longrightarrow G$ in (a) and $r_2: G_1 \longrightarrow G$ in (b) has no effect on the fundamental group.

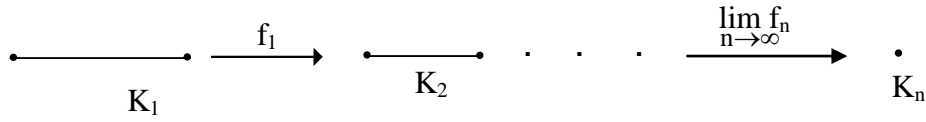
Now, we will study the simplicial complex and simplexes. From the definition of the simplex we have: The fundamental group of any n -simplex is zero, for all n .



Proposition 4: The fundamental group of the dynamical simplex to be a simplex after a time not changed.

Proof: If the variation of time does not accuse existence of loops in 1-simplexes or holes in n -simplex for $n \geq 2$, then the fundamental group has no change. Otherwise, the fundamental group changes.

(i) The folding of the dynamical 1-simplex K_1 , $f : K_1 \longrightarrow K_1$, $f(K_1) = K_2$.
 And the limit of folding which is the 0-simplex K_n , $\lim_{n \rightarrow \infty} f_n(K_1) = K_n$.



(a)

$$\pi(K_1) = \pi(K_2) = \pi(K_n) \cong 0.$$

The dynamical 1-simplex K which grows under the limit of variation of time t to be K_1 which is 2-simplex.

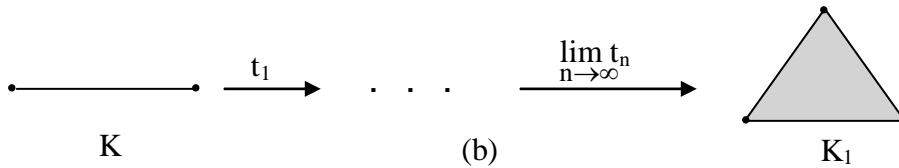


Fig. 8

$$\pi(K) = \pi(K_1) \cong 0.$$

(ii) The folding of the dynamical 2-simplex M , $f_1 : M \longrightarrow M$, $f_1(M) = M_1$
 and $f_2 : M_1 \longrightarrow M_1$, $f_2(M_1) = M_2$.

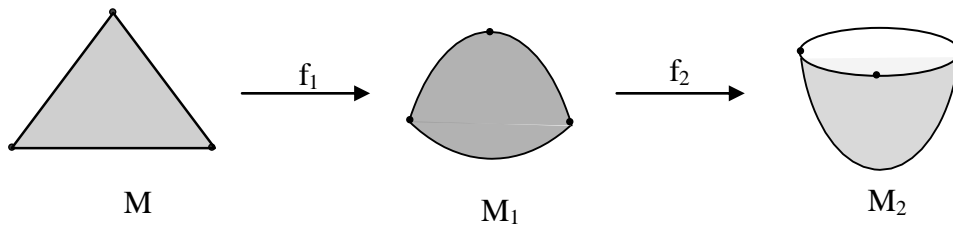


Fig. 9

$$\pi(M) = \pi(M_1) = \pi(M_2) \cong 0.$$

(iii) The limit of the unfoldings of the dynamical 2-simplex K , $\text{unf}: K \rightarrow K$.

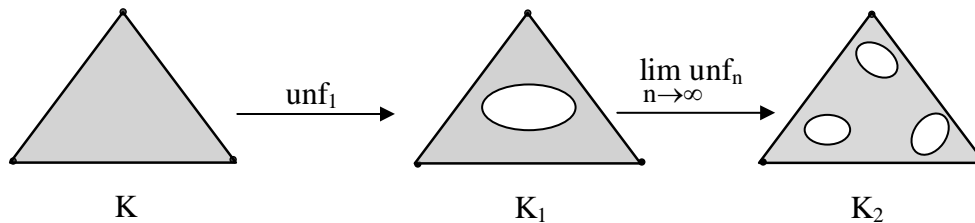


Fig. 10

$\pi(K) = 0$, but $\pi(K_1) = Z$, $\pi(K_2) = Z \oplus Z \oplus Z$. And also the limit of folding of K_2 which is the dynamical 2-simplex K .

REFERENCES

- 1 G. D. Birkhoof, Bull Am Math. Soc. 37 (1) (2000) 88.
- 2 J. Chaos Gleick, The Making of a New Science, Viking, New York, (1987).
- 3 K. T. Alligood, T. D. Sauer and J. A. Yorke, Chaos: An Introduction to Dynamical Systems, Springer-Verlag, New York, Heidelberg and Berlin, (1990).
- 4 D. Kaplan, L. Glass, Understanding Non-Linear Dynamics, Springer-Verlag, New York, Heidelberg and Berlin, (1995).
- 5 S. N. Rasband, Chaotic Dynamics of Non-Linear Systems, John Wiley and Sons, New York, (1989).
- 6 S. Wiggins, Introduction to Applied Non-Linear Dynamical System and Chaos, Springer-Verlag, New York, Heidelberg and Berlin, (1997).
- 7 M. El-Ghoul, Fuzzy Set Syst., 58 (1993) 355.
- 8 M. El-Ghoul and H. Shamara, Fuzzy Set Syst., (1997) 2336.
- 9 M. El-Ghoul, Aust Math J., (to be published).
- 10 M. El-Ghoul, Chaos Solutions and Fractal UK, 13 (2002) 833.

-
- 11 K. S. Sibirsky, **Introduction to Topological Dynamics**, Noordhoff Int. Pub. Leyden, The Netherlands, (1975).
 - 12 R. Balakrishnan, and K. Ranganthan, **A Text Book of Graph Theory**, Springer-Verlag, New York, (2000).
 - 13 W. S. Massy, **Algebraic Topology: An Introduction**, Harcourt, Brace and World, New York, (1967).
 - 14 S. A. Robertson, **Proc. Roy. Soc. Edinburgh**, (1977) 275.
 - 15 M. El-Ghoul, **Unfolding of Riemannian manifold**, Comm., Fac. Sci., A 37 (1988) 1.
 - 16 P. J. Giblin, **Graphs, Surfaces and Homology**, John Willey and Sons, New York, (1977).

ON s^*g -CLOSED SETS AND s^* -NORMAL SPACES

M. KHAN, *T. NOIRI AND **M. HUSSAIN

**Department of Mathematics, COMSATS Institute of Information Technology,
H-8/1, Islamabad, Pakistan

*2949-1 Shiokita-cho, Hinagu, Yatsushir- shi, Kumamoto-ken, 869-5142 Japan

E-mail Addresses: profmoiz001@yahoo.com, *t.noiri@nifty.com

**murad@comsats.edu.pk

(Received: February 08, 2009)

ABSTRACT: The notion of s^*g -closed sets in a topological space was introduced by Rao and Joseph [3]. In this paper, we show that the family of all s^*g -open sets in a topological space (X, \mathcal{T}) is a topology for X which is finer than \mathcal{T} . We introduce the notion of s^* -normal spaces and obtain some characterizations of s^* -normality and normality and some preservation theorems.

Keywords: g -closed sets, s^*g -closed sets, almost s^*g -continuous functions, almost s^*g -closed functions, s^* -normal space.

2000 AMS Classification: 54A05.

1. INTRODUCTION

The concept of closedness is fundamental with respect to the investigation of topological spaces. Levine [1] initiated the study of the so-called g -closed sets and by doing this he generalized the concept of closedness. The concept of g -closed sets was also considered by Dunham and Levine [2] in 1980. Recently, the notion of s^*g -closed sets in topological spaces has been introduced by Rao and Joseph [3]. An s^*g -closed set is also called ω -closed [4], g -closed [5] and s^*g -closed [6]. The notion of s^*g -closed sets is slightly stronger than that of g -closed sets and is properly placed between closed sets and g -closed sets. Moreover, s -normal (resp. semi-normal) spaces were introduced and studied by Maheshwari and Prasad [7] (resp. Dorsett [8]).

In this paper, we show that the family of all s^*g -open sets in a topological space (X, \mathcal{T}) is a topology for X which is finer than \mathcal{T} . We introduce the

notion of s^* -normal spaces which is stronger than both normality and semi-normality and obtain some characterizations of s^* -normality and normality and preservation theorems.

2. PRELIMINARIES

Throughout this paper, (X, \mathcal{F}) and (Y, σ) (or simply X and Y) will always denote topological spaces on which no separation axioms are assumed, unless otherwise mentioned. When A is a subset of X , $\text{cl}(A)$ and $\text{Int}(A)$ denote the closure and interior of a set A , respectively. A subset A of a topological space X is said to be α -open [9] (resp. semi-open [8]) if $A \subseteq \text{Int}(\text{cl}(\text{Int}(A)))$ (resp. $A \subseteq \text{cl}(\text{Int}(A))$). Moreover, A is said to be α -closed (resp. semi-closed) if $X \setminus A$ is α -open (resp. semi-open). $\text{SO}(X)$ (resp. $\text{SC}(X)$) represents the collection of all semi-open (resp. semi-closed) sets in X .

DEFINITION 2.1: Let X be a space. A subset A of X is said to be:

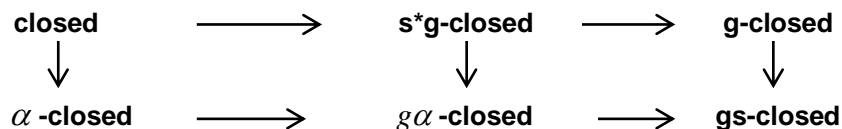
- 1) **generalized closed [1] (briefly, g-closed)** if $\text{cl}(A) \subseteq U$ whenever $A \subseteq U$ and U is open in X . The complement of a g-closed set is g-open;
- 2) **generalized semi-closed [10] (briefly, gs-closed)** if $\text{scl}(A) \subseteq U$ whenever $A \subseteq U$ and U is open in X . The complement of a gs-closed set is gs-open;
- 3) **generalized α -closed [11] (briefly, $g\alpha$ -closed)** if $\alpha\text{-cl}(A) \subseteq U$ whenever $A \subseteq U$ and U is α -open in X . The complement of a $g\alpha$ -closed set is $g\alpha$ -open.

3. s^*g -CLOSED SETS

DEFINITION 3.1: A subset A of a space X is said to be:

- 1) s^*g -closed [3] if $\text{cl}(A) \subseteq G$ whenever $A \subseteq G$ and G is semi open in X . The collection of all s^*g -closed subsets in X is denoted by $S^*GC(X)$. The intersection of all s^*g -closed sets containing A is denoted by $s^*g\text{-cl}(A)$.
- 2) s^*g -open if $X \setminus A$ is s^*g -closed, or equivalently, if $G \subseteq \text{Int}(A)$ whenever $G \subseteq A$ and G is semi closed in X . The collection of all s^*g -open subsets in X is denoted by $S^*GO(X)$.

REMARK 3.2: We summarize the fundamental relationships between several types of generalized closed sets in the following diagram. None of the implications is reversible.



Example 3.3: Let $X = \{a, b, c, d\}$ and $\mathcal{T} = \{\emptyset, X, \{a, b\}, \{a, b, c\}\}$. Then $\{a, b, d\}$ is a g -closed set which is not $g\alpha$ -closed.

Example 3.4: Let $X = \{a, b, c\}$ and $\mathcal{T} = \{\emptyset, X, \{a\}, \{b, c\}\}$. Then $A = \{a, c\}$ is an s^*g -closed set which is not α -closed.

Example 3.5: Let $X = \{a, b, c\}$ and $\mathcal{T} = \{\emptyset, X, \{a\}, \{a, b\}\}$. Then $A = \{b\}$ is an α -closed set which is not g -closed.

Theorem 3.6: The union of two s^*g -closed sets (and hence the finite union of s^*g -closed sets) in a space X is s^*g -closed.

Proof: Let G be a semi-open set containing $A \cup B$. Then $\text{cl}(A) \subseteq G$ and $\text{cl}(B) \subseteq G$ implies that $\text{cl}(A \cup B) \subseteq G$. This proves that $A \cup B$ is s^*g -closed.

Remark 3.7: Arbitrary union of s^*g -closed sets may not be s^*g -closed as shown by the following example.

Example 3.8: Let $X = \mathbb{N}$ and \mathcal{T} be the cofinite topology. Let $\{A_n : A_n = \{2, 3, \dots, n+1\}, n \in \mathbb{N}\}$ be a collection of s^*g -closed sets in X . Then $\bigcup_{n \in \mathbb{N}} A_n = \mathbb{N} \setminus \{1\} = A$ (say) having a finite complement is open and hence semi-open but not closed. As $\text{cl}(A) = \mathbb{N} \not\subseteq A$ gives, A is not s^*g -closed.

Definition 3.9: The intersection of all semi-open subsets of a space X containing a set A is called the semi kernel of A and is denoted by $s\text{ker}(A)$.

Lemma 3.10: A subset A of a space X is s^*g -closed if and only if $\text{cl}(A) \subseteq s\text{ker}(A)$.

Proof: Assume that A is an s^*g -closed set in X . Then $\text{cl}(A) \subseteq G$ whenever $A \subseteq G$ and G is semi-open in X . This implies $\text{cl}(A) \subseteq \bigcap \{G : A \subseteq G \text{ and } G \in \text{SO}(X)\} = s\text{ker}(A)$. For the converse, assume that $\text{cl}(A) \subseteq s\text{ker}(A)$. This implies $\text{cl}(A) \subseteq \bigcap \{G : A \subseteq G \text{ and } G \in \text{SO}(X)\}$. This shows that $\text{cl}(A) \subseteq G$ for all

semi-open sets G containing A . This proves that A is s^*g -closed.

Lemma 3.11: [9, Lemma 2] Every singleton $\{x\}$ in a space X is either nowhere dense or preopen.

Theorem 3.12: Arbitrary intersection of s^*g -closed sets in a space X is s^*g -closed.

Proof: Let $\{A_\alpha : \alpha \in I\}$ be an arbitrary collection of s^*g -closed sets in a space X and let $A = \bigcap_{\alpha \in I} A_\alpha$. Let $x \in \text{cl}(A)$. In view of Lemma 3.11, we consider the following two cases:

Case 1: $\{x\}$ is nowhere dense. If $x \notin A$, then for some $j \in I$, we have $x \notin A_j$. Since nowhere dense subsets are semi-closed [12, Theorem 1.3], therefore, $x \notin s\ker(A_j)$. On the other hand, by Lemma 3.10, since A_j is s^*g -closed, $x \in \text{cl}(A) \subseteq \text{cl}(A_j) \subseteq s\ker(A_j)$. By contradiction, $x \in A$ and hence $x \in s\ker(A)$.

Case 2: $\{x\}$ is preopen. Set $F = \text{Int}(\text{cl}(\{x\}))$. Assume that $x \notin s\ker(A)$. Then there exists a semi-closed set C containing x such that $C \cap A = \emptyset$. Now by [12, Theorem 1.2], $x \in F = \text{Int}(\text{cl}(\{x\})) \subseteq \text{Int}(\text{cl}(C)) \subseteq C$. Since F is an open set containing x and $x \in \text{cl}(A)$, therefore, $F \cap A \neq \emptyset$. Since $F \subseteq C$, $C \cap A \neq \emptyset$. By contradiction, $x \in s\ker(A)$. Thus in both cases $x \in s\ker(A)$. By Lemma 3.10, A is s^*g -closed.

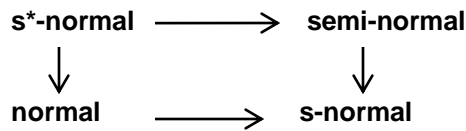
Corollary 3.13. For any space (X, \mathcal{F}) , $S^*GO(X)$ is a topology for X .

4. s^* -NORMAL SPACES

DEFINITION 4.1: A space X is said to be s -normal [7] (resp. semi-normal [8]) if for every pair of disjoint closed (resp. semi-closed) sets A and B in X , there exist disjoint semi-open sets U and V such that $A \subseteq U$ and $B \subseteq V$.

DEFINITION 4.2: A space X is s^* -normal if for each pair of disjoint semi-closed sets A and B , there exist disjoint open sets U and V such that $A \subseteq U$ and $B \subseteq V$.

REMARK 4.3: The following diagram holds. Since it is shown in [8, p.177] that normality and semi-normality are independent, none of the implications is reversible.



Theorem 4.4: For a topological space X , the following properties are equivalent:

- 1) X is s^* -normal;
- 2) for any disjoint $H, K \in \text{SC}(X)$, there exist disjoint s^* g-open sets U, V such that $H \subseteq U$ and $K \subseteq V$;
- 3) for any $H \in \text{SC}(X)$ and any $V \in \text{SO}(X)$ containing H , there exists an s^* g-open set U of X such that $H \subseteq U \subseteq s^*\text{g-cl}(U) \subseteq V$;
- 4) for any $H \in \text{SC}(X)$ and any $V \in \text{SO}(X)$ containing H , there exists an open set U of X such that $H \subseteq U \subseteq \text{cl}(U) \subseteq V$;
- 5) for any disjoint $H, K \in \text{SC}(X)$, there exist disjoint regular open sets U, V such that $H \subseteq U$ and $K \subseteq V$.

Proof: (1) \Rightarrow (2): Since every open set is s^* g-open, the proof is obvious.

(2) \Rightarrow (3): Let $H \in \text{SC}(X)$ and V be any semi-open set containing H . Then $H, X \setminus V \in \text{SC}(X)$ and $H \cap (X \setminus V) = \phi$. By (2), there exist s^*g -open sets U, G such that $H \subset U, X \setminus V \subset G$ and $U \cap G = \phi$. Therefore, we have $H \subset U \subset X \setminus G \subset V$. Since U is s^*g -open and $X \setminus G$ is s^*g -closed, we obtain $H \subset U \subset s^*g\text{-cl}(U) \subset X \setminus G \subset V$.

(3) \Rightarrow (4): Let $H \in \text{SC}(X)$ and $H \subset V \in \text{SO}(X)$. By (3), there exist an s^*g -open set U_0 of X such that $H \subset U_0 \subset s^*g\text{-cl}(U_0) \subset V$. Since $s^*g\text{-cl}(U_0)$ is s^*g -closed and $V \in \text{SO}(X)$, $\text{cl}(s^*g\text{-cl}(U_0)) \subset V$. Put $\text{Int}(U_0) = U$, then U is open and $H \subset U \subset \text{cl}(U) \subset V$.

(4) \Rightarrow (5): Let H, K be disjoint semi-closed sets of X . Then $H \subset X \setminus K \in \text{SO}(X)$ and by (4) there exists an open set U_0 such that $H \subset U_0 \subset \text{cl}(U_0) \subset X \setminus K$. Therefore, $V_0 = X \setminus \text{cl}(U_0)$ is an open set such that $H \subset U_0, K \subset V_0$ and $U_0 \cap V_0 = \phi$. Moreover, put $U = \text{Int}(\text{cl}(U_0))$ and $V = \text{Int}(\text{cl}(V_0))$, then U, V are regular open sets such that $H \subset U, K \subset V$ and $U \cap V = \phi$.

(5) \Rightarrow (1): This is obvious.

By using s^*g -open sets, we obtain a characterization of normal spaces.

Theorem 4.5: For a topological space X , the following properties are equivalent:

- 1) X is normal;
- 2) for any disjoint closed sets A and B , there exist disjoint s^*g -open sets U and V such that $A \subset U$ and $B \subset V$;
- 3) for any closed set A and any open set V containing A , there exists an s^*g -open set U of X such that $A \subset U \subset \text{cl}(U) \subset V$.

Proof: (1) \Rightarrow (2): This is obvious since every open set is s^*g -open.

(2) \Rightarrow (3): Let A be a closed set and V an open set containing A . Then A and $X \setminus V$ are disjoint closed sets. There exist disjoint s^*g -open sets U and

W such that $A \subset U$ and $X \setminus V \subset W$. Since $X \setminus V$ is closed, we have $X \setminus V \subset \text{Int}(W)$ and $U \cap \text{Int}(W) = \phi$. Therefore, we obtain $\text{cl}(U) \cap \text{Int}(W) = \phi$ and hence $A \subset U \subset \text{cl}(U) \subset X \setminus \text{Int}(W) \subset V$.

(3) \Rightarrow (1): Let A, B be disjoint closed sets of X . Then $A \subset X \setminus B$ and $X \setminus B$ is open. By (3), there exists an s^* -g-open set G of X such that $A \subset G \subset \text{cl}(G) \subset X \setminus B$. Since A is closed, we have $A \subset \text{Int}(G)$. Put $U = \text{Int}(G)$ and $V = X \setminus \text{cl}(G)$. Then U and V are disjoint open sets of X such that $A \subset U$ and $B \subset V$. Therefore, X is normal.

Theorem 4.6. Let X be an s^* -normal space. Then a semi-regular subspace Y of X is also s^* -normal.

Proof: Let X be an s^* -normal space and Y be a semi-regular subspace of X . Let $A \in SC(Y)$ and $B \in SO(Y)$ containing A . Since Y is semi regular, so $A \in SC(X)$ and $B \in SO(X)$. Hence by Theorem 4.4(4), there exists an open set U in X such that $A \subset U \subset \text{cl}_X U \subset B$. This gives $A \subset U \cap Y \subset \text{cl}_Y(U \cap Y) \subset B$, where $U \cap Y$ is open in Y and hence Y is s^* -normal.

5. FUNCTIONS AND S^* -NORMAL SPACES

DEFINITION 5.1: A function $f : X \rightarrow Y$ is said to be:

- 1) almost s^* -g-continuous if for any regular open set V of Y , $f^{-1}(V) \in S^*GO(X)$;
- 2) almost s^* -g-closed if for any regular closed set F of X , $f(F) \in S^*GC(Y)$.

DEFINITION 5.2: A function $f : X \rightarrow Y$ is said to be:

- 1) irresolute [13] (resp. semi-continuous [14]) if for any semi-open (resp. open) set V of Y , $f^{-1}(V)$ is semi-open in X ;

- 2) pre-semi-closed [15] (resp. semi-closed [16]) if for any semi-closed (resp. closed) set F of X , $f(F)$ is semi-closed in Y .

Theorem 5.3: A function $f : X \rightarrow Y$ is an almost s^*g -closed surjection if and only if for each subset S of Y and each regular open set U containing $f^{-1}(S)$, there exists an s^*g -open set V such that $S \subseteq V$ and $f^{-1}(V) \subseteq U$.

Proof: Necessity. Suppose that f is almost s^*g -closed. Let S be a subset of Y and U a regular open set of X containing $f^{-1}(S)$. Put $V = Y \setminus f(X \setminus U)$, then V is an s^*g -open set of Y such that $S \subseteq V$ and $f^{-1}(V) \subseteq U$.

Sufficiency: Let F be any regular closed set of X . Then $f^{-1}(Y \setminus f(F)) \subseteq X \setminus F$ and $X \setminus F$ is regular open. There exists an s^*g -open set V of Y such that $Y \setminus f(F) \subseteq V$ and $f^{-1}(V) \subseteq X \setminus F$. Therefore, we have $f(F) \supseteq Y \setminus V$ and $F \subseteq f^{-1}(Y \setminus V)$. Hence, we obtain $f(F) = Y \setminus V$ and $f(F)$ is s^*g -closed in Y . This shows that f is almost s^*g -closed.

Theorem 5.4: If $f : X \rightarrow Y$ is an almost s^*g -closed irresolute (resp. semi-continuous) surjection and X is s^* -normal, then Y is s^* -normal (resp. normal).

Proof: Let A and B be any disjoint semi-closed (resp. closed) sets of Y . Then $f^{-1}(A)$ and $f^{-1}(B)$ are disjoint semi-closed sets of X . Since X is s^* -normal, there exist disjoint open sets U and V of X such that $f^{-1}(A) \subseteq U$ and $f^{-1}(B) \subseteq V$. Put $G = \text{Int}(\text{cl}(U))$ and $H = \text{Int}(\text{cl}(V))$, then G and H are disjoint regular open sets of X such that $f^{-1}(A) \subseteq G$ and $f^{-1}(B) \subseteq H$. By Theorem 5.3, there exist s^*g -open sets K and L of Y such that $A \subseteq K$, $B \subseteq L$, $f^{-1}(K) \subseteq G$ and $f^{-1}(L) \subseteq H$. Since G and H are disjoint, K and L are

also disjoint. It follows from Theorem 4.4 (resp. Theorem 4.5) that Y is s^* -normal (resp. normal).

Theorem 5.5: If $f : X \rightarrow Y$ is a continuous almost s^* g-closed surjection and X is a normal space, then Y is normal.

Proof: The proof is similar to that of Theorem 5.4.

Theorem 5.6: If $f : X \rightarrow Y$ is an almost s^* g-continuous pre-semi-closed (resp. semi-closed) injection and Y is s^* -normal, then X is s^* -normal (resp. normal).

Proof: Let H and K be disjoint semi-closed (resp. closed) sets of X . Since f is a pre-semi-closed (resp. semi-closed) injection, $f(H)$ and $f(K)$ are disjoint semi-closed sets of Y . Since Y is s^* -normal, there exist disjoint open sets P and Q such that $f(H) \subset P$ and $f(K) \subset Q$. Now, put $U = \text{Int}(\text{cl}(P))$ and $V = \text{Int}(\text{cl}(Q))$, then U and V are disjoint regular open sets such that $f(H) \subset U$ and $f(K) \subset V$. Since f is almost s^* g-continuous, $f^{-1}(U)$ and $f^{-1}(V)$ are disjoint s^* g-open sets such that $H \subset f^{-1}(U)$ and $K \subset f^{-1}(V)$. It follows from Theorem 4.4 (resp. Theorem 4.5) that X is s^* -normal (resp. normal).

REFERENCES

1. N. Levine, Rend. Circ. Mat. Palermo (2), 19 (1970) 89.
2. W. Dunham and N. Levine, Kyungpook Math. J., 20 (1980) 169.
3. K. C. Rao and K. Joseph, Bull. Pure Appl. Sci., 19 (E)(2) (2002) 281.
4. P. Sundaram and M. Sheikh John, Proc. 82nd Indian Science Congress, Calcutta, (1995).
5. M. K. R. S. V. Kumar, Ind. J. Math., 43(2) (2001) 231.
6. M. Murugalingam, A Study of Semi Generalized Topology, Ph.D. Thesis, Manonmaniam Sundaranar Univ., Tirunelveli Tamil Nadu, India, (2005).
7. S.N. Maheshwari and R. Prasad, Bull. Math. Soc. Sci. Math. R. S.

-
- Roumanie (N.S.), 22(70) (1978) 27.
8. C. Dorsett, *Kyungpook Math. J.*, 25 (1985) 173.
 9. D. S. Janković and I. L. Reilly, *Ind. J. Pure Appl. Math.*, 16(9) (1985) 957.
 10. S. P. Arya and T. M. Nour, *Ind. J. Pure Appl. Math.*, 21 (1990) 717.
 11. H. Maki, R. Devi and K. Balachandran, *Bull. Fukuoka Univ. Ed. Part III*, 42 (1993) 13.
 12. S. G. Crossley and S. K. Hilderband, *Texas J. Sci.*, 22 (1971) 99.
 13. S. G. Crossley and S. K. Hilderband, *Fund. Math.*, 74 (1972) 233.
 14. N. Levine, *Amer. Math.*, 70(1) (1963) 36.
 15. G. L. Garg and D. Sivaraj, *Period. Math. Hungar.*, 19 (1988) 97.
 16. T. Noiri, *Atti Accad. Naz. Lincei Rend. Cl. Sci. Fis. Mat. Natur.* (8), 54 (1993) 412.

THE EFFECT OF FLUORINE DOPING ON OPTOELECTRONIC PROPERTIES OF TIN-DIOXIDE (F: SnO₂) THIN FILMS

S. A. YOUSAF AND S. ALI

Department of Physics, GC. University, Lahore, Pakistan
Correspondance Author: salamatali@gcu.edu.pk

(Received: September 21, 2009)

ABSTRACT: Fluorine Doped Tin dioxide (F: SnO₂) Thin Films are a special kind of material that exhibit electrical conductivity and at the same time transmittance in visible region making it suitable for Solar Cell applications. To study the effect of doping on optical and conducting properties of F: SnO₂ thin films, a series of investigations were made. The thin films were deposited on a glass substrate from SnCl₄.5H₂O and HF in 2-propanol with different concentration of fluorine, utilizing a sol-gel dip-coating technique. The effect of doping concentration during deposition reaction influences the crystal growth; electrical and optical properties are presented and discussed. The XRD analysis reveals the perfect substitution of doped atoms with host atoms for low concentration while deteriorating crystal structure for higher concentration. The four point probe method showed that resistivity is varying for different concentration ratios from 120 Ω-m for un-doped film and decreased to one order of magnitude to 0.358 Ω-m for 1:40 atomic ratio as the optimum ratio for Fluorine doping. The transmittance has inverse effect with F concentration and remains almost constant in the visible region for each concentration, which make it suitable for solar cell applications. The band gap calculations showed that the increase in band gap with increased doping concentration could be due to increase in n-type carrier concentration, as the absorption edge shifts to higher energy level.

Keywords: Fluorine Doped Tin dioxide (F: SnO₂), Dip-coating Technique, Solar Cell, Electrical Conductivity, Transmittance and Band gap.

1. INTRODUCTION

Fluorine doped Tin dioxide Thin Films belong to a special class of metal oxide thin films i.e. Transparent Conducting Oxide Thin Films which are a special part of nanostructured thin film solar cells. It offers the possibility of fabrication of low cost solar cells. As it permits the transmission of solar

radiation directly to the active region with little or no attenuation, these solar cells have improved sensitivity in the high-photon-energy portion of the solar spectrum and make thin film solar cells suitable for large scale application with high performance efficiency [1].

It is a well known fact that materials which show high electrical conductivity are usually almost opaque to the visible light due to their high absorption coefficient and/or reflectivity, whereas transparent materials are usually insulating or semiconducting owing to lack of free carriers at ambient temperatures. But in Transparent Conducting Oxides (TCO), the coexistence of electrical conductivity and optical transparency is achieved by selecting a wide-band gap metal oxide that is rendered degenerate through the introduction of native or substitution dopants [2]. It also depends on the nature, number and atomic arrangements of metal cations in crystalline or amorphous oxide structures, on the morphology, and on the presence of intrinsic or intentionally introduced defects. These Metal Oxide thin films are prepared under controlled environment; the resulting films are n-type degenerated semiconductors with free electron concentrations of the order of 10^{20} cm^{-3} provided by native donors such as oxygen vacancies: as oxygen vacancy provides a pair of electron and enhances the conduction [3]. However, since un-doped oxide films were found to be unstable when used at high temperature, metal oxides without impurity doping have not proved feasible as practical transparent electrodes [3]. Another advantage of using impurity doped materials is that they can use both native and impurity donors. F, Cl, Sb, Br, Ni, Cu are few of the examples which can be used as dopant for SnO_2 . Among them F: SnO_2 and Sb: SnO_2 have been studied a lot and employed for device applications. Sb atoms substitute Sn where F atoms sit in the place of Oxygen. There is a clear indication from the hybrid orbital configuration of $2s^2 2p^5$ and $2s^2 2p^4$ for F and O, respectively that F atoms give one free electron/molecule when F sits in the place of oxygen. The ionic radii of F (1.36 \AA) is slightly lower than that of O^{2-} (1.40 \AA) so that doping takes place easily [4].

Due to these advantages, F: SnO₂ thin films with varying concentration of F, were chosen to investigate for its optoelectronic properties, so that it could be used for solar cell applications with enhanced efficiency.

2. DEPOSITION PROCEDURE

The experimental procedure to deposit the thin films comprised of two steps:

Cleaning of Glass Slides:

For thin film deposition we used glass slides as substrates. The glass slides were cut into pieces of 1x 1.5 inch and then cleaned ultrasonically at 60°C following different steps.

Deposition of F: SnO₂ thin films:

SnCl₄ .5H₂O and HF were taken as starting materials and 2-propanol as solvent for tin chloride. 0.5M solutions of both were mixed, refluxed and stirred at 70°C for 1 hr and then aged for 2 hrs. After aging, ultrasonically cleaned glass slides were dipped in the solution 10 times and between each two dips dried at 90°C. These slides were then annealed in oxygen controlled environment at 500°C and then taken out at 300°C to allow sudden cooling of the material. The whole procedure has been depicted in Fig. 1. Using this procedure we deposited different thin films on the glass substrate with varying Fluorine, Tin dioxide atomic ratios of 1:60, 1:40, and 1:35 while one slide was prepared with pure Tin dioxide for comparison.

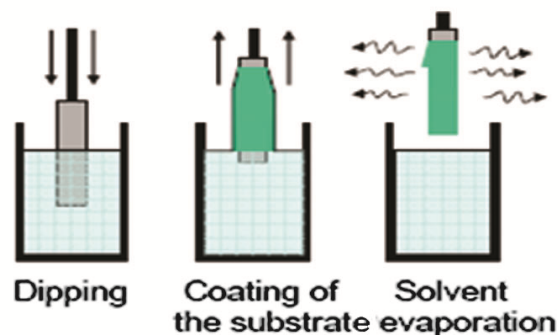


Fig. 1: The process of sol-gel dip coating

3. RESULTS AND DISCUSSION

3.1 STRUCTURAL ANALYSIS:

To find the structure, composition and phases present in the fabricated samples, XRD model MPD X'PERT PRO of PANalytical Company Ltd., Holland, using $\text{CuK}\alpha$ as characteristic radiation ($\lambda = 0.15418 \text{ nm}$) with $\theta - \theta$ configuration was used. The measurements were made in 2θ ranging from 20° to 80° . Analysis was mainly done by the software X'Pert High Score of the same Company.

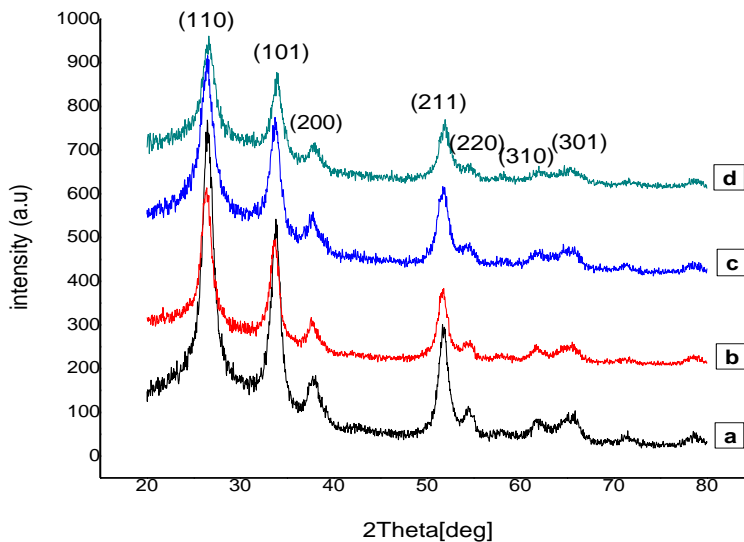


Fig. 2: Combined XRD Pattern of 4 Samples where (a) un-doped SnO_2 (b) F: SnO_2 with atomic ratio 1:60 (c) F: SnO_2 with atomic ratio 1:40 (d) F: SnO_2 with atomic ratio 1:35.

Fig. 2 shows the X-ray Diffraction pattern of different samples of SnO_2 thin films (without background correction). The peaks are identified to originate from (110), (101), (200), (211), (220), (310), (301) reflections of tetragonal SnO_2 crystal structure [5].

All the films exhibit the preferred orientation along (110) plane which is

also observed by other groups with SnO₂: F grown by dip coating technique [6]. As we can see, there are no additional peaks in doped profile which is the evidence of perfect substitution of doped atoms with host atoms. It is also observed that as the doping concentration increases, the intensity of peaks decreases which is because at higher doping concentration the crystal structure starts to deteriorate [7].

3.2 OPTICAL ANALYSIS:

A Spectrophotometer model HR2000CG-UV-NIR was used to obtain transmission spectrum in visible region. Fig. 3 represents the Transmittance Spectrum of samples in the Visible Region. It is evident from the graph that as the doping concentration increases transmittance decreases, which is probably due to the increase in fundamental absorption as photon striking increases with increase in carrier concentration [7].

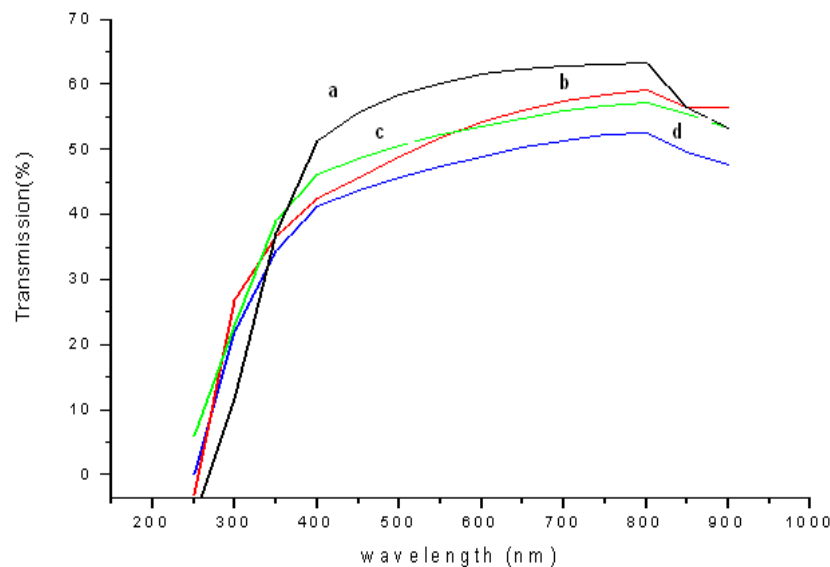


Fig. 3: Transmission Spectrum in Visible Region (a) un-doped SnO₂ (b) F: SnO₂ with atomic ratio 1:60 (c) F: SnO₂ with atomic ratio 1:40 (d) F: SnO₂ with atomic ratio 1:35.

The transmission data of Fig. 3 have been used to calculate the band gap using equation

$$(\alpha h\nu)^2 = A(h\nu - E_g)$$

where A is a constant, $h\nu$ is the photon energy, E_g is the energy band gap and α is the absorptivity. The plot between $(\alpha h\nu)^2$ and $h\nu$ is shown in Fig. 4.

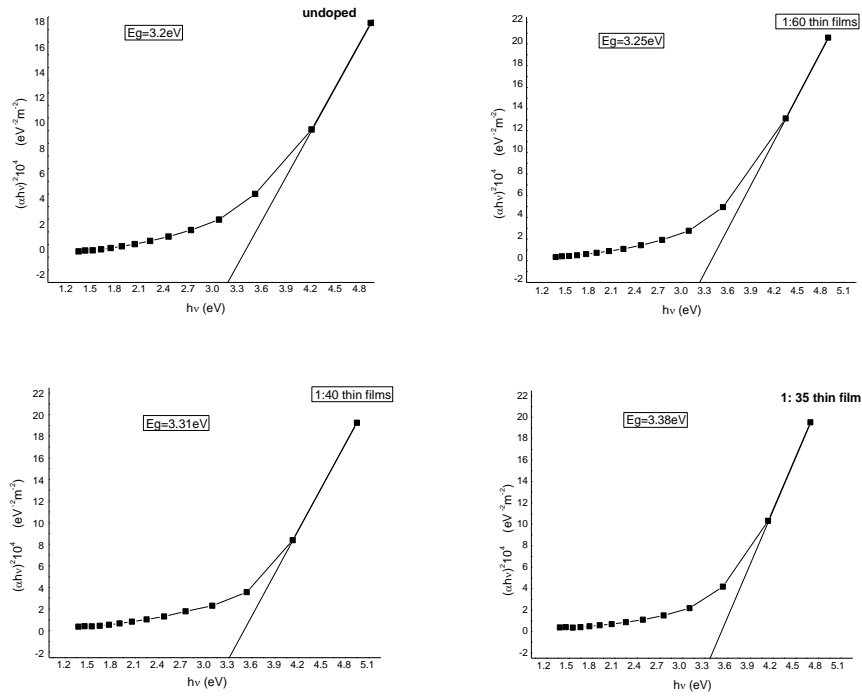


Fig. 4: Band gap calculation; Data of Fig. 3 has been used to draw $(\alpha h\nu)^2$ versus $h\nu$.

By extrapolating the linear portion of the graph to $h\nu$ axis, band gap have been obtained at the intercept [6]. Table 1 gave the evidence that band gap value increases with increase in doping concentration, which could be due to the Burstein-Moss Shift [8] i.e. due to increase in carrier concentration, the absorption edge shifts to higher energy level.

Table 1: Atomic Ratios of F in SnO_2 versus Band Gap E_g

No.	Sample	Band gap, E_g (eV)
1	Undoped	3.23
2	1:60	3.28
3	1:40	3.4
4	1:35	3.42

3.3 ELECTRICAL ANALYSIS

The Electrical Resistance test was done using Four Point Probe Method. The results are shown in Table 2. It can be seen here that initially with doping, electrical resistance decreases due to increase in no. of charge carriers. But as we kept on increasing the doping concentration, at a point resistance increases again. This is due to the fact that at higher concentration, Fluorine atoms incorporates at the interstitial sites and crystal structure of the films start to deteriorate (as shown in XRD pattern), hence decreases the mobility of the free electrons and increases the electrical resistivity [8].

Table 2: Atomic Ratios of F in SnO₂ versus Electrical Resistivity.

No.	Sample	Electrical Resistivity (Ω -m)
1	Un-doped	1.20
2	1:60	6.41×10^{-01}
3	1:40	3.58×10^{-01}
4	1:35	4.60×10^{-01}

4. CONCLUSIONS

F: SnO₂ thin films have successfully been fabricated using sol-gel dip coating technique. It has been observed that with increasing doping concentration, there is a decrease in crystalline structure, electrical resistance and optical transmission. But at limiting doping concentration optoelectronic properties stop being improved.

REFERENCES

1. A. L. Dawar and J. C. Joshi, J. Mat. Sci., 19 (1984) 1.
2. P. P. Edwards, A. Porch, M. D. Jones, D. V. Morgan and R. M. Perks, Dalton Trans., (2004) 2995.
3. T. Minami, MRS Bulletin 25(8) (2000) 38.
4. K. S. Ramaih and V. S. Raja, Appl. Sur. Sci., 253 (2006) 1451.
5. W. H. Baur, Acta Crystallographica, 9(6) (1956) 515.
6. A. N. Banerjee, S. Kundoo, P. Saha and K. K. Chattopadhyay, J. Sol-Gel Sci. and Tech., 28 (2003) 105.

7. S. Shanthi, C. Subramanian and P. Ramsamy, *Mat. Sci. and Engg.*, B 57 (1999) 127.
8. H. Kim, R. C. Y. Auyeung and A. Pique, *Thin Solid Films*, 516 (2008) 5052.

EFFECT OF PARTICLE SIZE ON THE STRUCTURAL AND TRANSPORT PROPERTIES of $\text{La}_{0.67}\text{Ca}_{0.33}\text{MnO}_3$ NANOPARTICLES

M. Z. IQBAL, S. ALI AND M. A. MIRZA

Department of Physics, GC University, Lahore, Pakistan

Corresponding Author: salamatali@gcu.edu.pk

(Received: October 19, 2009)

ABSTRACT: The effect of nanometric particle size on structural and transport properties of single phase, nanocrystalline, granular $\text{La}_{0.67}\text{Ca}_{0.33}\text{MnO}_3$ (LCMO) is investigated. The materials were synthesized using the *modified citrate route* by sintering at five different temperatures starting from 600 to 1000 °C, with an interval of 100 °C. XRD analysis showed that the particle size increases with the increase in sintering temperature. A systematic study of electrical resistivity of all five samples was undertaken as a function of temperature (80–300 K). The metal-insulator transition temperature (T_P) was determined, which increases (from 114 to 193 K) with increase in sintering temperature. Most interestingly, transport measurements show that with the increase in annealing temperature, the effect gets more pronounced with the increase in particle size. These transport measurements were counterchecked by magnetic (AC susceptibility) and thermal (Differential Scanning Calorimeter (DSC)) measurements and found in good agreement with each other. The core-shell model has been applied to the data for theoretical explanation.

Keywords: *Colossal magnetoresistance, Nanoparticles, Modified Citrate Route, Structural Property, Transport Properties, Magnetic and Thermal properties, Core-Shell Model.*

1. INTRODUCTION

Transitional-metal oxides (TMO) with the perovskite structure have a long history of research and have been known as materials with a variety of interesting properties such as structural, electrical transport and magnetic properties. The first renewal of interest in the perovskite (TMO) took place when the high-temperature superconducting (high- T_C) cuprates with layered perovskite structures were discovered [1]. The second renewal [2] was brought in by the important recent activities on mainly perovskite

manganites of the form $Re_xAe_{1-x}MnO_3$ where, $Re=La, Sm, Nd, Pr$.(trivalent rare-earth ions) and $Ae= Ca, Sr, Ba$.(divalent alkaline-earth ions). Intensive studies of the colossal magnetoresistance (CMR) in this class of materials have been carried out in case of single crystals[3,4] and ceramic CMR materials [5,6] for both the search of the correct model to explain their structural and transport properties and the possible application of them as magnetic sensors and magnetic data storage devices.

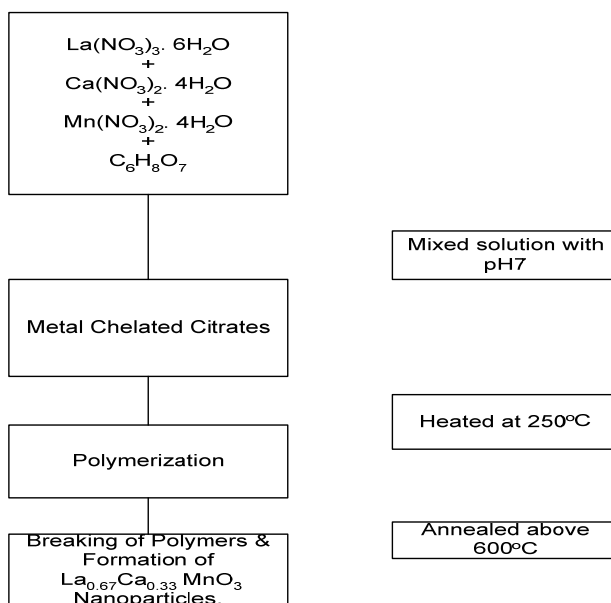
The simplest explanation of the CMR observed for the *manganites* around ferromagnetic-paramagnetic Curie temperature (T_C) is given in terms of the double-exchange (DE) model. However, the physics of the extraordinary magnitude of CMR is obviously more complex. There are other important factors than in the above simplest DE scenario, e.g., electron-lattice interaction, antiferromagnetic superexchange interaction between the t_{2g} local spins, intersite exchange interaction between the e_g orbitals (orbital ordering tendency), intrasite and intersite Coulomb repulsion interactions among the e_g electrons, etc. [7].

A number of such investigations of the grain size (in the nanometric regime) effect on electrical transport properties of perovskites $La_{1-x}A_xMnO_3$ have been recently published [8-19]. Nevertheless, no definitive theory or understanding has yet been achieved regarding the nanosize effect on various physical properties of *manganites*. The proper physical explanation for large discrepancies between metal-insulator transition temperature T_P and ferromagnetic-paramagnetic transition temperature T_C and the gradual drop of T_P with decrease in grain size while T_C remains almost constant, in the case of a nanomanganite system, still is a matter of debate. Detailed investigations are required to explain the grain size effect on the temperature dependent behavior, which is very much essential from the technological perspective. In the case of nanodimensional system, several extrinsic effects dominate over that of intrinsic properties of the system, so it can be readily understood that the preparation procedure must have a profound influence on its physical properties. In fact, the preparation

procedure determines the nature of the surface region of nanosize grains, which plays a very crucial role in electrical transport behavior of nanodimensional systems.

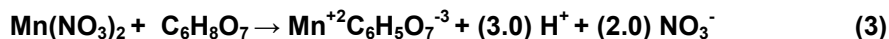
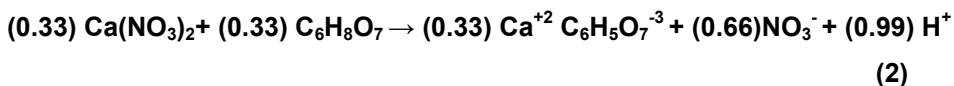
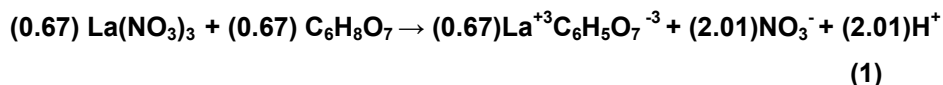
2. EXPERIMENTAL DETAILS

The single-phase, nanocrystalline samples of $\text{La}_{0.67}\text{Ca}_{0.33}\text{MnO}_3$ were synthesized by a variant of sol-gel technique known as *Modified Citrate Route*. We take stoichiometric proportions of $\text{La}(\text{NO}_3)_3 \cdot 6\text{H}_2\text{O}$, $\text{Ca}(\text{NO}_3)_2 \cdot 4\text{H}_2\text{O}$ and $\text{Mn}(\text{NO}_3)_2 \cdot 4\text{H}_2\text{O}$ as starting materials (all having 99.9% purity). All these reactants were dissolved in distilled water and mixed in 2 molar solution of citric acid with mild stirring. After half an hour aqueous lanthanum-calcium-manganese-citrate formed [20-23]. Ethanol was used for precipitation. A drop-wise addition of aqueous metal citrate solution into ethanol causes rapid precipitation to provide a fine and homogenous citrate precursor which leads to the formation of mixed phase of LCMO and heated at 100°C to evaporate the water. After heating at 100°C , a light pink powder is formed. The powder was heated at 250°C for polymerization for 6h, resulted in a highly porous black powder. Powder was separated into parts and annealed for 5h at 600°C , 700°C , 800°C , 900°C and 1000°C to produce samples of different particle sizes. The reaction scheme is shown below:

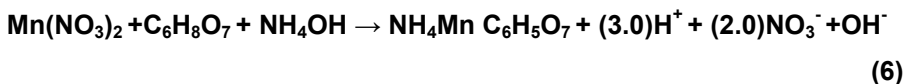
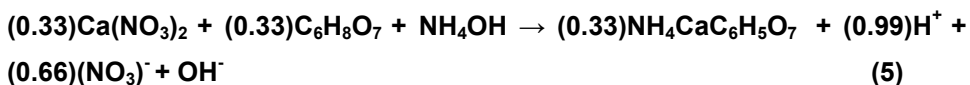
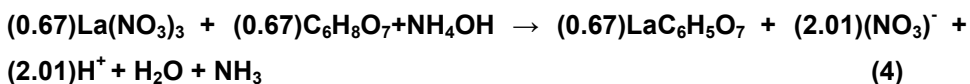


Concentration of citric acid

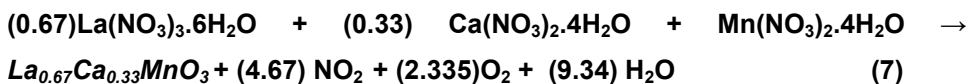
From the following equations, we can determine the concentration of citric acid:



On addition of NH_4OH above products as shown in equations (1) to (3) become as follows:



The final equation is given below:



3. RESULTS AND DISCUSSION

1. X-ray diffraction

Powder X-ray diffraction (XRD) data were recorded and collected on the XRD model MPD X'PERT PRO of PANalytical Company Ltd., Holland, using $\text{CuK}\alpha$ as characteristic radiation ($\lambda = 0.15418\text{nm}$) with $\theta - \theta$ configuration. The measurements were made in 2θ ranging from 20° to 70° . Analysis was mainly done by the software X'Pert HighScore of the same Company. The XRD data shows that these peaks match those for the compound of the same composition, i.e. $\text{La}_{0.67}\text{Ca}_{0.33}\text{MnO}_3$. The standard peak position is present at 23.19° , 32.55° , 40.23° , 46.74° , 58.32° , 68.73° . It is clear from Fig.1 that the peak width increases with the decreases of annealing temperature, which is an indication of particle size decrease with the decrease of annealing temperature. Also peaks seem to be slightly shifted towards 32.89 which imply that the particle becomes more crystallized as the annealing temperature increases.

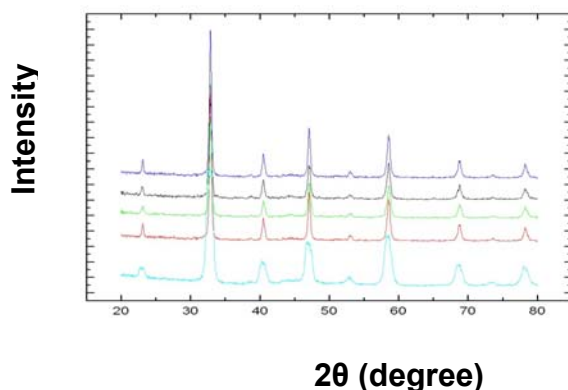


Fig. 1: XRD Pattern for samples annealed at different temperatures.

Table 1: Particle Size Variation with Annealing Temperature.

Annealing Temperature (°C)	Particle Size (nm)
600	21
700	26
800	32
900	38
1000	46

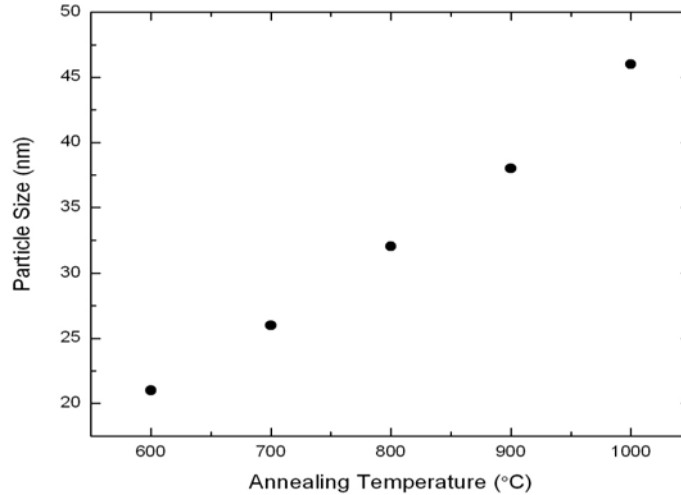


Fig. 2: Particle size vs Annealing temperature

The particle size of each sample was determined from the x-ray data using Scherer's formula. The effect of particle size with increase in annealing temperature has been tabulated in Table 1 and shown in Figure 2. In heating process when the particles are formed, they collide and either coalesce with one another to form a larger particle or coagulate. The process which occurs depends upon the temperature and available energy, that's why particle size increases with increasing temperature.

2. Transport, Thermal and Magnetic Properties

Resistivity measurements of all the samples were carried out over a temperature range (80–300K) on the setup designed locally and the results are presented in Figure 3 and tabulated in Table 2. The typical compound $\text{La}_{0.67}\text{Ca}_{0.33}\text{MnO}_3$ is a ferromagnetic metal at low temperature regime and shows interesting transport properties at the nanoscale. The electrical resistivity ρ_T of $\text{La}_{0.67}\text{Ca}_{0.33}\text{MnO}_3$ nanoparticles annealed at temperatures 600°C , 700°C , 800°C , 900°C and 1000°C was measured by four probe method. All the resistivity data were recorded during heating the samples. It is observed from the resistivity data of Figure 3, that T_P (Peak Temperature or Metal-Insulator transition temperature) increases with the increase in annealing temperature. Data of Table 2 confirmed this trend. All these results have been plotted in Figures 4 and 5.

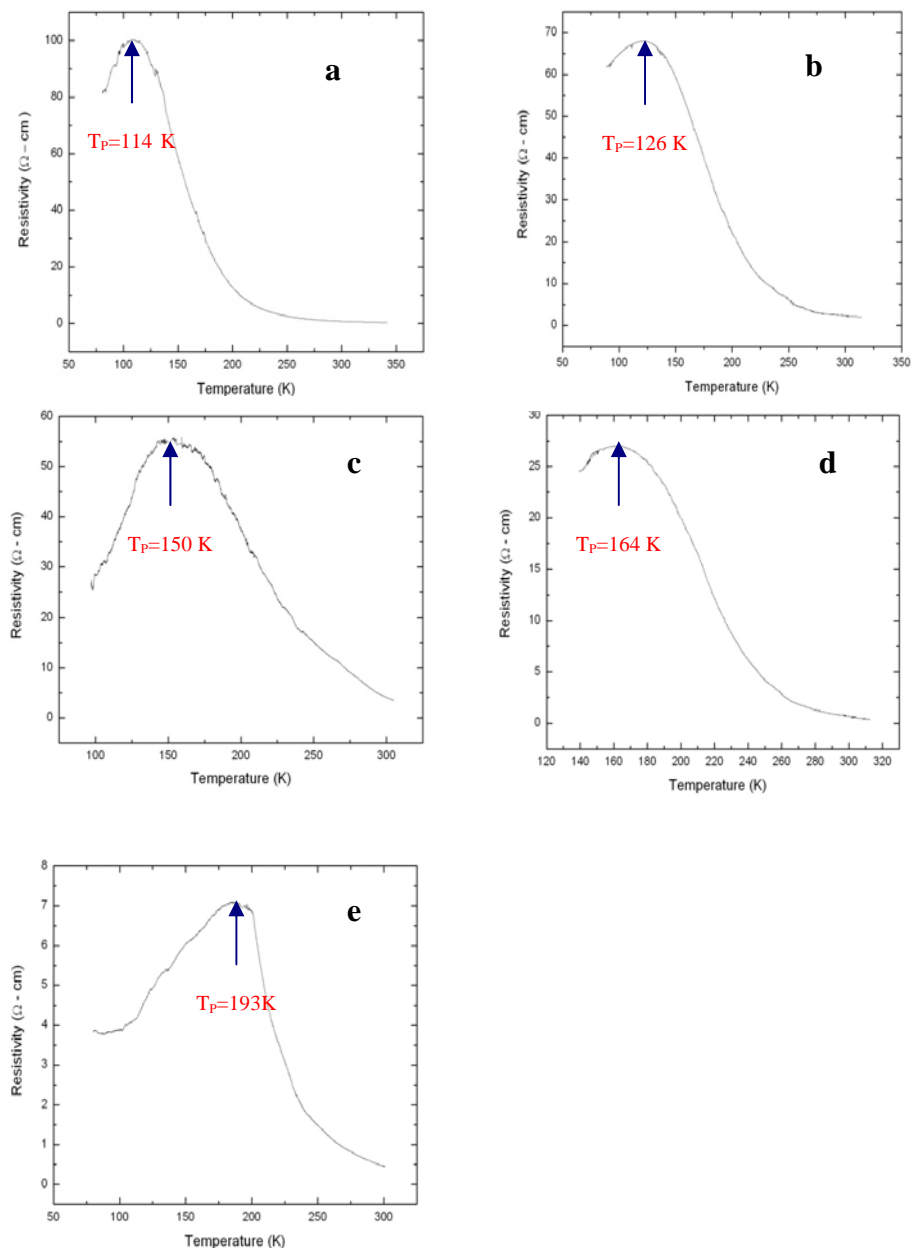


Fig. 3: Resistivity of samples vs. Annealed Temperature at: a) 600 °C, b) 700 °C, c) 800 °C, d) 900 °C and e) 1000 °C

The arrow indicates the Transition Temperature T_p . The increase in T_p is evident with increase in Annealing Temperature.

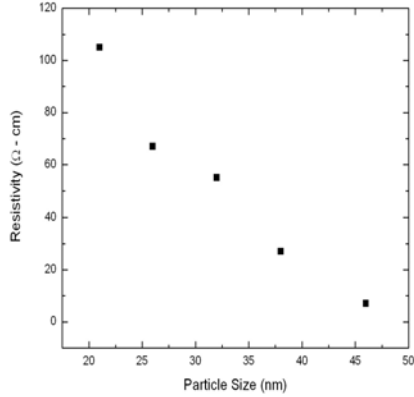


Fig. 4: Particle Size vs Resistivity (at T_p)

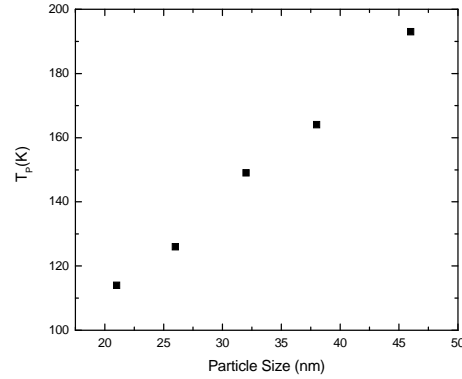


Fig. 5: Particle Size vs T_p (Metal-Insulator transition temperature)

Table 2: The experimental data of LCMO nanoparticle materials.

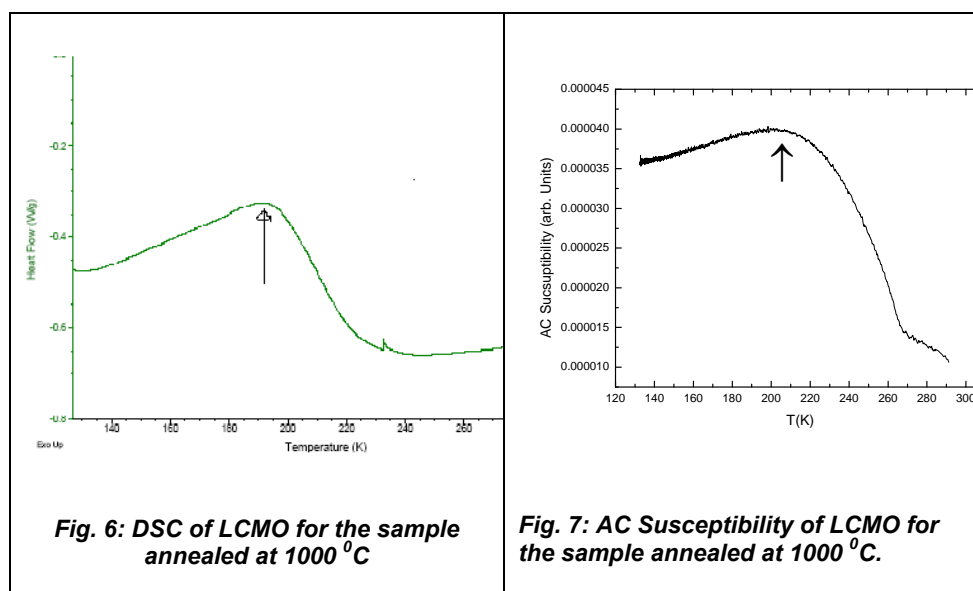
Sample Code	Compositional Formula	Annealing Temperature (°C)	Peak-Temperature (T_p) (K)	Resistivity at T_p $P_{(Peak)}$ (Ω cm)
LCMO-6	$La_{0.67}Ca_{0.33}MnO_3$	600	114	105
LCMO-7	$La_{0.67}Ca_{0.33}MnO_3$	700	126	67
LCMO-8	$La_{0.67}Ca_{0.33}MnO_3$	800	149	55
LCMO-9	$La_{0.67}Ca_{0.33}MnO_3$	900	164	27
LCMO-10	$La_{0.67}Ca_{0.33}MnO_3$	1000	193	07

A Low Temperature Differential Scanning Calorimeter (DSC) Q200 of TA Instrument, USA was used to confirm the phase transition in these materials at the mentioned temperature as shown in Figure 6.

The magnetic phase transition from the ferromagnetic FM to paramagnetic PM state in the $La_{0.67}Ca_{0.33}MnO_3$ system represents a signal, which is more than 50 times weaker than the melting of Gallium. $La_{0.67}Ca_{0.33}MnO_3$ (LCMO) was chosen since it is considered to be one of the possible candidate refrigerants in the field of room-temperature magnetic refrigeration and has a transition just around 235 K depending on the exact way of synthesizing

and heat treatment. Figure 6 shows the results of DSC on a 5 mg LCMO sample (annealed at 1000°C) with heating rate of 10 K/min. The calorimetric result has also been confirmed by AC susceptibility measurement on the same sample as shown in Figure 7. In AC susceptibility measurement on doped manganese oxides indicates that the entropy of the sample has been changed a lot under the magnetic field. With decreasing temperature the sample undergoes a FM transition near T_p as indicated in Figures 6 & 7 by the arrows. The spontaneous magnetic ordering with the variation of temperature may also affect the lattice and, entropy, which is reflected by the peak of specific heat near T_c as shown in Fig 6.

In view of these observations, there is a tremendous influence of crystallite size on various properties mentioned and the observed behavior can be explained on the basis of a qualitative model called Core Shell Model [24]. According to core-shell model, when the grain size of the material is decreased, a non-magnetic surface layer having nanocrystalline size would be created around the grain. This may increase the residual resistivity of the material, which in turn decreases the density of Ferromagnetic metallic (FMM) particles. Therefore, lowering of T_p and enhancement of electrical resistivity at a given temperature ρ_T are expected. Finally, shifting of T_p



towards low-temperature region is to the loss of long-range ferromagnetic order of the sample [25]. The particle size decreases with the decrease in T_p . This may be due to the fact that small size particles having different oxygen stoichiometry affecting T_p . As the oxygen content reduces T_p also reduces. The decrease in resistivity with the increase of annealing temperature defects lead to the decrease and resistivity will also decrease, which is also reported [26].

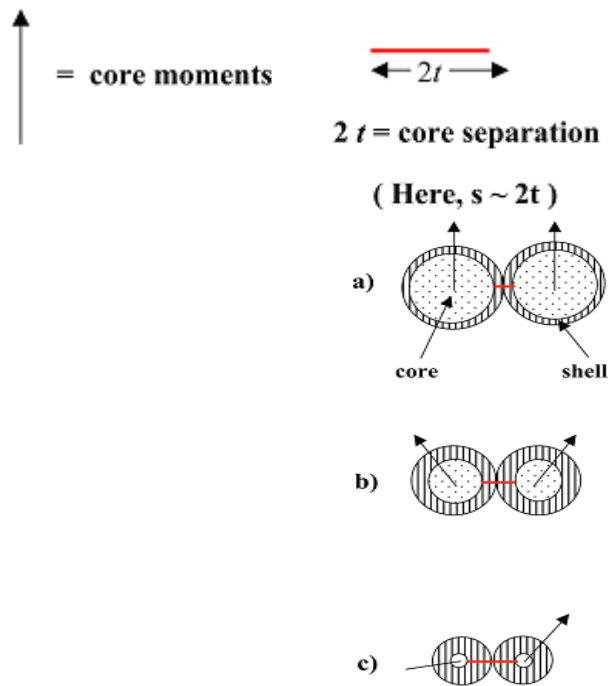


Fig. 8: The possible ordering of core moments in the core-shell structure of nanometric manganite grains

The effect of decrease in resistivity can be explained by assuming that when the size of the manganite grain reduces to few tens of nanometers, in core-shell structure, where the inner part of the grain, i.e. the core, would have the same properties as the bulk compound whereas the outer layer i.e. shell width t , would contain most of the oxygen defects and faults in the crystallographic structure, which would lead to a magnetically dead layer. It is a quite well-established fact that shell thickness ' t ' increases with the decrease in grain size [27,28,29]. Basically, the net intercore barrier

thickness ($s=2t+d$), namely the total shell thickness $2t$ of two neighboring grains together with the intergranular distance d increases with the reduction of grain size. The schematic diagram in Fig.8 shows that with the decrease in grain size core separation ($s \approx 2t$) increases significantly with the thickness of the shell t , even if we consider the grains to be in intimate contact $d=0$ for all grain size samples. For polycrystalline CMR samples having an average grain size larger than 100 nm, d is reported [1] to be 1-2 nm (where $t \approx 0$). 't' to be about 2 nm in magnitude for a manganite samples having a minimum grain size of 50 nm i.e in that case, even if we consider two grains to be in intimate contact $d=0$, ($s \approx 2t$) will be 4 nm[27]. We are working in the range of 21- 46 nm, thus in our case effective 's' is expected to be several nanometers. Even for our largest grain 46 nm sample, 's' is expected to be reasonably greater than 4 nm. Another important fact is that in absence of magnetic field the contributory portion of each individual grain to the magnetization is the core and not the shell. According to core-shell model, nanoparticle has a core (inner volume) in which magnetic moments are regularly aligned and a shell (surface region) in which defects are present and moments are not regularly aligned. By decreasing particle size the surface to volume ratio increases and surface effects become prominent at the nanometer scale and the resistivity continuously decreases with the increase of annealing temperature, which conforms from core-shell model.

4. CONCLUSIONS

The single phase LCMO with different nanometer size particles has been fabricated using a special experimental procedure (the *modified citrate route*). The XRD analysis has provided the crystallite size (particle size). The effect of particle size on transport properties has been studied at length. The Metal-Insulator along with Ferro-Paramagnetic transition has been studied and confirmed by Magnetic and Thermal measurements. The qualitative core-shell model has been applied on this data for the theoretical explanation of these phenomena.

5. ACKNOWLEDGEMENTS

This work was supported by the Higher Education Commission of Pakistan under the Project Grant No. 1109 and Pakistan Science Foundation under the Project No. Phy-246.

REFERENCES

1. J. G. Bednorz and K. A. Muller, *Z. Phys. B: Condens. Matter*, **64** (1986) 189.
2. R. von Helmolt, J. Wecker, B. Holzappel, L. Schultz and K. Samwer, *Phys. Rev. Lett.*, **71** (1993) 2331.
3. J.S. Zhou, J. B. Goodenough, A. Asamitsu and Y. Tokura, *Phys. Rev. Lett.*, **79** (1997) 3234.
4. R. A. Rao, D. Lavric, T. K. Nath, C. B. Eom, L. Wu and F. Tsui, *Appl. Phys. Lett.*, **73** (1998) 3294.
5. R. Mahendiran, S. K. Tiwary, A. K. Raychaudhuri, T. V. Ramakrishnan, R. Mahesh, N. Rangavittal and C. N. R. Rao, *Phys. Rev.*, **B 53** (1996) 3348.
6. H. Y. Hwang, S.W. Cheong, P. G. Radaelli, M. Marezio and B. Batlogg, *Phys. Rev. Lett.*, **75** (1995) 914.
7. Y. Tokura (Ed.), *Colossal Magnetoresistive Oxides*, Gordon and Breach New York, (2000).
8. J. Rivas, L. E. Hueso, A. Fondado, F. Rivadulla and M. A. López-Quintela, *J. Magn. Magn. Mater.*, **221** (2000) 57.
9. D. G. Lamas, A. Caneiro, D. Niebieskikwiat, R. D. Sánchez, D. García and B. Alascio, *J. Magn. Magn. Mater.*, **241** (2002) 207.
10. N. Zhang, W. Ding, W. Zhong, D. Xing and Y. Du, *Phys. Rev.*, **B 56** (1997) 8138.
11. M. M. Savosta, V. N. Krivoruchko, I. A. Danielenko, V. Y. Tarenkov, T. E. Konstantinova, A. V. Borodin and V. N. Varyukhin, *Phys. Rev.*, **B 69** (2004) 024413.
12. L. Balcells, B. Martínez, F. Sandiumenge and J. Fontcuberta, *J. Magn. Magn. Mater.*, **211** (2000) 193.
13. T. Zhu, B. G. Shen, J. R. Sun, H. W. Zhao and W. S. Zhan, *Appl.*

-
- Phys. Lett., 78 (2001) 3863.
14. Y. W. Duan, X. L. Kou and J. G. Li, *Physica, B* 355 (2005) 250.
 15. Tianhao Ji, Jiye Fang, Volodymyr Golob, Jinke Tang, and Charles J. O'Connor, *J. Appl. Phys.*, 92 (2002) 6833.
 16. A. Dutta, N. Gayathri and R. Ranganathan, *Phys. Rev.*, B 68 (2003) 054432.
 17. R. Mahesh, R. Mahendiran, A. K. Raychaudhuri and C. N. R. Rao, *Appl. Phys. Lett.*, 68 (1996) 2291.
 18. R. D. Sánchez, J. Rivas, C. Vázquez-Vázquez, A. López-Quintela, M. T. Causa, M. Tovar and S. Oseroff, *Appl. Phys. Lett.*, 68 (1996) 134.
 19. L. E. Hueso, F. Rivadulla, R. D. Sánchez, D. Caeiro, C. Jardón, C. Vázquez-Vázquez, J. Rivas and M. A. López-Quintela, *J. Magn. Magn. Mater.*, 189 (1998) 321.
 20. L. W. Tai and P. A. Lessing, *J. Mater. Res.*, 7 (1992) 502.
 21. L. W. Tai and P. A. Lessing, *J. Mater. Res.*, 7 (1992) 511.
 22. V. K. Sankaranarayanan, Q. A. Pankhurst, D. P. E. Dickson and C. Johnson, *J. Magn. and Magn. Mater.*, 73 (1993) 120.
 23. E. Zhecheva, R. Stoyanova, M. Gorava, R. Alcantara, J. Mortalez and J. R. Tirado, *Chem. Mater.*, 8 (1996) 1429.
 24. P. Dey, T. K. Nath, *Phy. Rev.*, B, 73 (2006) 214425.
 25. S. L. Yuan, M. H. Liu, Z. Y. Li, G. Peng, Z. C. Xia, Y. P. Yang, F. Tu, G. Q. Zhang, J. Liu, L. Liu, J. Tang, G. H. Zhang, W. Feng, C. S. Xiong and Y.H. Xiong, *Solid State Commun.*, 121 (2002) 291.
 26. F. Rivadulla, L. E. Hueso, J. Rivas, M. C. Blanco, M. A. Lopez-Quintela and R. D. Sanchez, *J. Magn. and Magn. Mater.*, 203 (1999) 253.
 27. N. Zhang, W. Ding, W. Zhong, D. Xing and Y. Du, *Phys. Rev.*, B 56 (1997) 8138.
 28. T. Zhu, B. G. Shen, J. R. Sun, H. W. Zhao and W. S. Zhan, *Appl. Phys. Lett.*, 78 (2001) 3863.
 29. L. I. Balcells, J. Foncuberta, B. Martínez and X. Obradors, *Phys. Rev.*, B 58 (1998) R14697.

VARIATION OF ION ENERGY FLUX WITH INCREASING WORKING GAS PRESSURES USING FARADAY CUP IN PLASMA FOCUS DEVICE

H. A. R. TARIQ, I. A. KHAN, U. IKHLAQ AND A. HUSSNAIN

Department of Physics, GC University, Lahore, Pakistan
Corresponding author: ejaz_phd@yahoo.com (I.A. Khan)

(Received: February 06, 2010)

ABSTRACT: Faraday Cup is used to estimate the ion energy flux with various working gas (nitrogen) pressures (0.75 mbar, 1 mbar and 1.25 mbar) in the chamber of plasma focus device. Faraday Cup is placed at 4 cm from the tip of anode at 67° with respect to anode axis to detect the ions. The estimated ion energy for various pressures is found to be 3.23 KeV, 3.5KeV and 12KeV respectively using the time of flight method. Ion flux varies from 4.34×10^{16} - 1.86×10^{17} ions/sterad for energy range (3.23 KeV to 12 KeV). Results show that maximum ion flux is obtained for ions of lower energies while minimum ion flux is obtained for ions of higher energies. The focusing efficiency of plasma focus device depends on working gas pressures and it is found that good focus is achieved for higher (1.25 mbar) pressure comparatively resulting in the emission of higher energetic ions. Thus ion energy flux is associated with the focusing efficiency of plasma focus device as well as working gas pressures.

Keywords: Plasma focus; Ion energy flux; Angular positions

1. INTRODUCTIONS

Plasma focus (PF) is a simple and cost effective device. It has attracted much attention as an intense and pulsed source of x-rays [1, 2], neutrons [3] and beams of energetic ions and relativistic electrons [4, 5]. Due to its simplicity, it is being used for diverse applications like x-rays and electron beams lithography [1, 6], x-rays backlighting [7], radiography of biological specimens [8] and deposition of composite films such as ZrN, ZrON, ZrAlON, ZrCN, (Ti/Si) N and carbonitriding of silicon [9-14]. Results show that different properties of the deposited films are attributed to ion energy flux. Thus, ion energy flux plays a key role to deposit smooth and uniform films of diverse properties. It has been reported that ion energy flux is

maximum (40 keV to 1.2 MeV) when the detector is placed along the anode axis [9]. It has also been reported that ion energy flux decreases with increasing detector angular positions [15]. Thus it was necessary to characterize the ion energy flux emitted during the radial collapse phase of PF operation by placing the detector at higher degree angular positions. The present work shows the estimation of ion energy flux when the detector is placed at 4 cm from the anode but at 67° angular position with respect to anode axis, which is to confirm the variation in ion energy flux at higher angular positions.

2. EXPERIMENTAL SET UP

A schematic diagram of PF device, which is used as source of energetic ions and relativistic electrons, is shown in Figure 1. It is a Mather type PF device energized by a single capacitor (32 μ F, 15 kV) [16]. The electrode system consists of a copper anode surrounded by six equidistant copper rods forming a cathode. The anode is engraved 15 mm deep at the tip to reduce the copper impurities [17]. A Pyrex glass insulator sleeve is placed between the electrodes to facilitate the formation of current sheath. The electrode assembly is housed in a stainless steel vacuum chamber, which is evacuated by a rotary vane pump down to the pressure (gas nitrogen) of 1 Pa (10^{-2} mbar). A triggertron type pressurized spark gap switch is used to transfer energy from the capacitor to the electrodes. The total parasitic inductance of the system is about 80 nH. The focusing efficiency is monitored by using Tektronix (TDS 3054B 500 MHz) Oscilloscope through a high voltage probe while the discharge current is recorded using a Rogowski coil. The details of the PF facilities can be found elsewhere [9, 16].

The parametric characterization of the nitrogen ions is performed by employing a Faraday Cup placed at 4 cm above the tip of anode and at 67° angular position with respect to anode axis. The velocity, energy and total number of nitrogen ions (ions flux) emitted from the focus region are calculated using the time of flight (TOF) technique [17]. PF device is

operated for different working gas (nitrogen) pressures (0.75 mbar, 1 mbar and 1.25 mbar) in order to find the effect of pressures on velocity, energy and flux of ions.

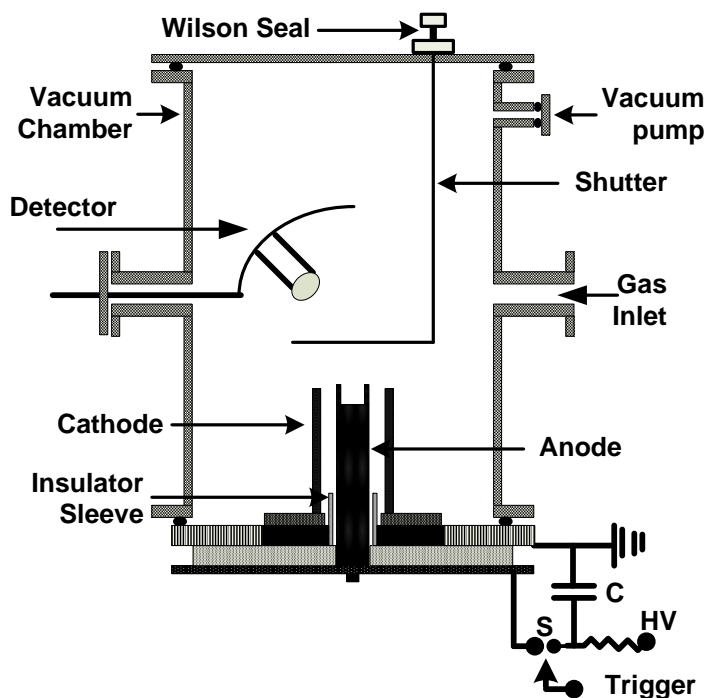


Fig. 1: Schematic diagram of PF device

3. RESULTS AND DISCUSSION

Faraday Cup is used to estimate the ion energy flux emanated during the radial collapse phase of plasma focus operation. Ion beam signals are recorded for different (0.75 mbar, 1 mbar and 1.25 mbar) filling gas pressures using Faraday Cup when placed at 4 cm from the anode tip but at 67° with respect to anode axis. High voltage probe signals for different (mentioned above) working gas pressures are also recorded in order to determine the focusing efficiency of the device.

Fig. 2 exhibits a typical ion beam along with high voltage signals recorded with Faraday Cup and high voltage probe for 1.25 mbar pressure

respectively. Intense peak of high voltage probe signal for 1.25 mbar pressure indicates a good focusing resulting in the emission of more energetic ions. However, it is clear that ion beam signal consists of two peaks, first corresponds to x-rays while the second peak relates to the desired ion beam pulse since the ions are massive thereby reaching the detector late.

The velocity of nitrogen ions is estimated by taking the ratio of the distance to the flight time of ions from the source to the detector. Flight time is estimated by correlating the ion beam pulse with the x-ray pulse emitted due to the intense electric field produced during the radial collapse phase of plasma focus operation. The estimated ion velocity is thus used to calculate the energy of ions reaching the detector using the following expression:

$$E = \frac{1}{2}mv^2$$

where m is the atomic mass of nitrogen ions.

The estimated velocity and energy of ions are thus found to be 21 cm/ μ s, 22 cm/ μ s, 40 cm/ μ s, 3.23 KeV, 3.5 KeV and 12 KeV for different (0.75, 1.0, 1.25 mbar) pressures respectively.

Ion flux is evaluated by employing the spectral law [18]:

$$\frac{dN}{dE} = \alpha E^{-X}$$

where N is the total number of ions having energy E (keV), the exponent X is in the range 2-5 and α is the proportionality constant which is equal to 1.12×10^{19} a.u.. To determine the ion flux, we integrate the above equation between the limits E_1 to E_2 and the number of ions with energy in this interval can thus be obtained as

$$N(E) = \frac{\alpha}{-x+1} [E_1^{-x+1} - E_2^{-x+1}]$$

where E_1 and E_2 are low and high limits of energy corresponding to given energy interval.

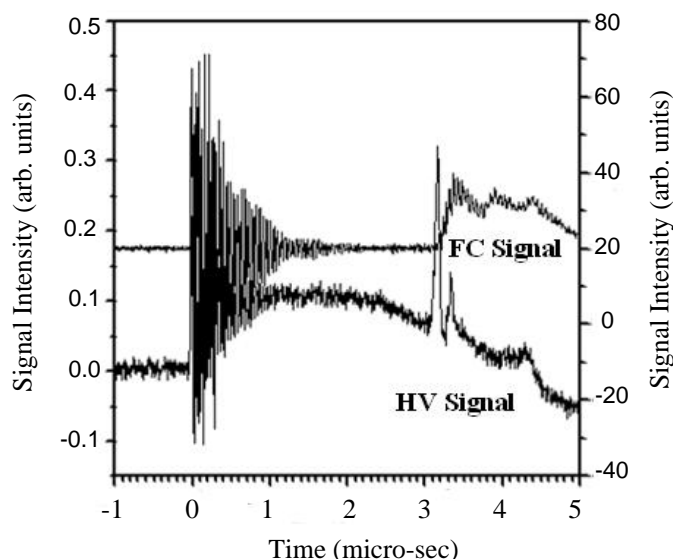


Fig. 2: Typical ion beam signal recorded with Faraday Cup and high voltage signal recorded with high voltage probe

Figure 3 shows the ions flux as function of ion energy. It is clear that ion flux decreases with the ion energy. It is maximum (1.86×10^{17} ion/sterad) for lower (3.23 keV) ion energy and minimum (4.34×10^{16} ion/sterad) for higher ion energy (12 keV). Thus ions flux varies from 1.86×10^{17} to 4.34×10^{16} ion/sterad for different (0.75, 1.0, 1.25 mbar) working gas pressures.

For (0.75 mbar) pressure, the electric field produced during the radial collapse phase of plasma focus operation is not so intense which results in the emission of low velocity ions. Therefore low energy ions are emitted. These low energy ions easily travel to reach the detector due to low pressure of working gas resulting in high ions flux to the detector. For (1 mbar) pressure, the electric field is comparatively better which gives ions of higher velocity and energy but due to higher pressure, lesser number of ions can thus reach at the detector resulting in lower ions flux. For (1.25 mbar) pressure, strong electric field is produced which results in the emission of ions of higher velocity and energy but due to higher pressure, again lesser number of ions can thus reach at the detector resulting in lowest ions flux. Thus it is concluded that the focusing efficiency of the

device, ions velocity and ions energy increase with the increase of working gas pressure. This indicates that ions velocity and ions energy totally depend on the focusing efficiency of the plasma which in turn depends on the intense electric field developed during the radial collapse phase of plasma focus device.

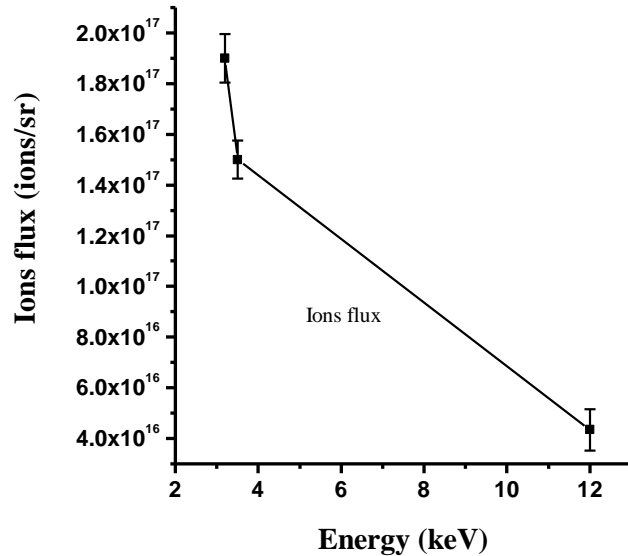


Fig. 3: Variation of ions flux as function of ions energy.

It has been reported that ions energy is maximum (40 keV to 1.2 MeV) when the detector (BPX65 photodiode) was placed along the anode axis [9]. In the present study, the detector is placed at 67° and ions energy is found to be 12 keV for the same (1.25 mbar) working gas pressure. This result confirms that ions energy flux decreases with the increase of detector angular positions. These characteristic ions of different energies and flux are being used to deposit composite films of diverse properties. Thus low energy ions and lesser ions flux might give the smooth surface because higher ions energy gives comparatively rough and damaged surfaces due to the sputtering.

4. CONCLUSIONS

PF is a rich source of energetic ions and relativistic electrons and x-rays. Energy of ions emanating from hot plasma column depends on the

focusing efficiency of the device and the detector angular positions with respect to anode axis. Faraday Cup placed at 67° angular position from the anode axis is used to estimate ions energy and flux. Time of flight technique is used to estimate the velocity of ions reaching the detector surface. The focusing efficiency of the device increases with the increase of working gas (nitrogen) pressure. Ions velocity and energy also increase (3.23 KeV to 12 KeV) with the increase of working gas (0.75, 1.0 and 1.25 mbar) pressures. The ions flux (1.86×10^{17} — 4.34×10^{16} ion/sterad) is decreased with working gas pressure. Ions take more time to reach the detector under high pressure due to more collisions.

REFERENCES

1. Y. Kato, I. Ochiai, Y. Watanabe and S. Murayama, *J. Vac. Sci. Technol.*, B 6 (1988) 195.
2. R. Lebert, W. Keff and D. Rothweiler, *J. X-ray Sci. Technol.*, 6 (1996) 107.
3. H. Asai and I. Ueno. *Fusion Engineering and Design*, 7 (1989) 335.
4. W. Harries L, J. H. Lee and D. R. Mcfarland, *Plasma Phys.*, 20 (1978) 95.
5. J. R. Smith, C. M. Luo, M. J. Rhee and R. F. Schneider, *Phys. Fluids*, 28 (1985) 2305.
6. P. Lee, X. Feng, G. X. Zhang, M. H. Liu and S. Lee, *Plasma Sources Sci. Technol.*, 6 (1997) 343.
7. M. Zakauallah, K. Alamgir, M. Shafiq, M. Sharif and A. Waheed, *IEEE Trans. Plasma Sci.*, 30 (2002) 2089.
8. M. F. Castillo, M. M. Milanese, R. L. Moroso, J. O. Pouzo and M. A. Santiago, *IEEE Trans. Plasma Sci.*, 29 (2001) 921.
9. I. A. Khan, M. Hassan, R. Ahmad, A. Qayyum, G. Murtaza, M. Zakauallah and R. S. Rawat, *Thin Solid Films*, 516 (2008) 8255.
10. I. A. Khan, M. Hassan, R. Ahmad, G. Murtaza, M. Zakauallah, R. S. Rawat and P. Lee, *Inter. J. Mod. Phys.*, B 22 (23) (2008) 3941.
11. I. A. Khan, M. Hassan, T. Hussain, R. Ahmada, M. Zakauallah and R. S. Rawat, *Appl. Surf. Sci.*, 255 (2009) 6132.

12. I. A. Khan, S. Jabbar, T. Hussain, M. Hassan, R. Ahmad, M. Zakaullah and R.S. Rawat, Nucl. Instru. Meth. Phys. Res., B 268 (2010) 2228.
13. T. Hussain, R. Ahmad, I. A. Khan, J. Siddiqui, N. Khalid, A. S. Bhatti and S. Naseem, Nucl. Instru. Meth. Phys. Res., B, 267 (2009) 768.
14. S. Jabbar, I. A. Khan, R. Ahmad, M. Zakaullah and J. S. Pan, J. Vac. Sci. Technol., A 27 (2) (2009) 381.
15. I. Bertalot and H. Herold, Phys. Lett., A 79 (1980) 389.
16. M. Hassan, R. Ahmad, A. Qayyum, G. Murtaza, A. Waheed and M. Zakaullah, Vacuum, 81 (2006) 291.
17. C. S. Wong, P. Choi, W. S. Leong and J. Singh, Japan. J. Appl. Phys., 41 (2002) 3943.
18. H. Kelly, A. Lepone, A. Marquez, D. Lamas and C. Oviedo, Plasma Sources Sci. Technol., 5 (1996) 704.

UNIAXIALLY STRAINED Si/SiGe HETEROSTRUCTURES

A. R. KHAN

Physics Department, Govt. M.A.O. College, Lahore Pakistan
Corresponding Author: aaliya.rehman@gmail.com

(Received: September 23, 2010)

ABSTRACT: Although, biaxial strained silicon (sSi) has received substantial attention over the past few years, however, little attention has been paid to uniaxial sSi. The most effective way to enhance hole mobility in FET devices is to introduce uniaxial tensile strain [1]. While high biaxial tensile strain is achieved by growing sSi on relaxed silicon germanium (SiGe) layers, a different approach has to be taken for uniaxial strain [2]. The amount of uniaxial strain required compared to biaxial strain is less by several orders of magnitude producing the same improvement factor.

Keywords: X-ray diffraction; semi-conductors; bi-axial strain

1. INTRODUCTION

Technology has come a long way from the fabrication of the wheel to fabrication of integrated circuits [3]. In the recent past, performance in metal-oxide semiconductor field-effect transistors (MOSFETs) has been improved vastly by reducing dimensions of the device gate and the thickness of the gate oxide. However, due to physical and economic limitations, further scaling is no longer practically beneficial and search continues for novel solutions.

Strain improves the drive currents in the channels by introducing changes in the band structure which in turn enhance the device performance, even at decidedly small channel lengths. For example, a relaxed $\text{Si}_{1-x}\text{Ge}_x$ graded buffer layer creates a larger lattice constant on a Si substrate which can act as a virtual substrate for further growth of biaxially tensile Si-rich layers or biaxially compressive Ge-rich layers. These $\text{Si}_{1-x}\text{Ge}_x$ virtual substrates enable the subsequent growth of thin layers which when strained can

confine holes or electrons. These heterostructures have improved mobility over that of bulk Si for both electrons and holes by a factor of ≈ 2 and ≈ 10 respectively.

2. EARLY WORK

The ground-work towards the exploitation of lattice mismatch in SiGe heterostructures was initiated by People et al. [4] who observed a two dimensional hole gas (2DHG) in strained Silicon (s)Si_{0.8}Ge_{0.2} layers grown on Si substrates having type-I band offset. However, no confinement for electrons was evident and it was inferred that ΔE_v is much greater than ΔE_c for s Si_{1-x}Ge_x grown on Si [4, 5]. Slightly enhanced electron mobilities were seen for Si/Si_{0.85}Ge_{0.15} superlattices fabricated on Si [6] depicting that tensile sSi when grown on partially or fully relaxed Si_{1-x}Ge_x alloys forms a type-II band offset thereby confining electrons [7]. It was observed that in a two-dimensional electron gas (2DEG) the sixfold-degenerate conduction band breaks into the lower energy twofold ($\Delta 2$ out-of-plane) valleys and fourfold ($\Delta 4$ in-plane) valleys at higher energy. Electron mobility was further improved by varying layer thicknesses and refining modulation-doping techniques [8, 9].

For the reduction of crystalline defects, research continued on pseudomorphically strained Si_{1-x}Ge_x heterostructures with Ge content less than 50 % grown on Si [5] and paved the way for the first SiGe heterojunction bipolar transistor [10] and SiGe p-channel FETs [11, 12]. The fabrication of relaxed Si_{1-x}Ge_x buffers vastly reduced threading dislocation densities [13, 14, 15]. Compositional grading is still considered the best technique for attaining completely relaxed Si_{1-x}Ge_x alloys with low density of defects grown on a Si substrate. For gaining more insight into the dislocations in mismatched semiconductor heteroepitaxy, one can refer to the following articles [16, 17, 18].

The sSi having type-II band offset was further utilized to create modulation-doped n-FETs having metal gates and buried channels [19, 20, 21], with the improvement that sSi surface channel n-FETs with SiO₂ gates were

introduced which could exhibit a 70 % higher effective mobility μ_{eff} than bulk Si n-MOSFETs [22]. By combining modulation doping and oxide-gated surface-channel transistors, band-engineered SiGe heterostructures have better performance prospects for digital applications [23]. A further step towards enhanced μ_{eff} was taken with the introduction of sSi p-MOSFET [24] wherein the strain induced breaking of the heavy-hole (hh) - light-hole (lh) degeneracy could be utilized to develop a p-MOSFET with greater μ_{eff}

3. CONTEMPORARY WORK

During the same period, work on extremely high mobility 2DHG in strained Ge(sGe) grown on $\text{Si}_{1-x}\text{Ge}_x$ ($x = 0.6$ to 0.7) virtual substrates and high transconductance sGe p-channel modulation-doped FETs (p-MODFETs) led to such $\text{Si}_{1-x}\text{Ge}_x$ heterostructures where tensile strained Si could become a channel for high-mobility electrons while compressively strained Ge could serve as a channel for high-mobility holes [25, 26]. A further step was the fabrication of Ge-rich ($\text{Si}_{1-y}\text{Ge}_y$) layers ($y = 0.55$ to 0.8) grown on relaxed $\text{Si}_{1-x}\text{Ge}_x$ [$y > x$] for attaining high hole mobilities even in the presence of alloy scattering [27]. Room-temperature hole mobilities of $105\text{cm}^2/\text{V s}$ ($3500\text{cm}^2/\text{V s}$ at 77 K) for $\text{sSi}_{0.2}\text{Ge}_{0.8}$ on relaxed $\text{Si}_{0.7}\text{Ge}_{0.3}$ were seen and it was demonstrated that high hole mobility is achievable even in Ge-rich strained alloys.

The research on the consequences of strain on mobility of electrons [23] and of holes [28] showed that by fabricating sSi n-MOSFETs on $\text{Si}_{1-x}\text{Ge}_x$ with $x = 0.10$ to $x = 0.37$, the enhancement factor for electrons reached maximum at 1.83 for ≈ 20 percent Ge in the $\text{Si}_{1-x}\text{Ge}_x$ but the hole mobility increases approximately linearly for same range of Ge content. However, at ambient temperatures, peak mobility improvement of 40 % in sSi p-MOSFETs was achieved [29]. Regarding hole mobility enhancement, double heterostructures were fabricated which consisted of a $\text{sSi}_{0.17}\text{Ge}_{0.83}$ layer sandwiched between a relaxed $\text{Si}_{0.52}\text{Ge}_{0.48}$ virtual substrate and a 5 nm of sSi cap layer. Enhancements in μ_{eff} by factors of 4 to 5 were attained [30], reaching a peak room-temperature μ_{eff} of $760\text{ cm}^2/\text{V}$

s [31, 32].

4. LATER AND RECENT WORK

The turn of the century saw an acceleration in research and development of MOSFETs based on SiGe with higher p-channel μ_{eff} and the introduction of several "on-insulator" technologies. For example, silicon-on-insulator (SOI)-based devices differ from conventional silicon-built devices in that the silicon junction is above an electrical insulator, typically silicon dioxide, for improved performance and diminished short channel effects in microelectronics devices. Early in 2001, fabrication of SiGe -on-insulator (SGOI) substrates with $x = 0.25$ was achieved by using the technique of wafer bonding of graded buffers with oxidized Si wafers [33, 34]. This technique greatly improved the electron mobility in the sSi layers grown subsequently. Among a few new methods, one was to transfer the relaxed layer of a $\text{Si}_{1-x}\text{Ge}_x$ buffer to a Si wafer via layer exfoliation [33]. Since the SiGe layer was peeled off (or split off) the substrate, it caused damages to the surface. The damaged surface was then smoothed and then another sSi top layer was grown. High mobility sSi n-MOSFETs were fabricated with higher Ge content through compositional grading and wafer bonding [33, 35, 36]. A thorough study of sSi n- and p-MOSFETs [37] discusses growth parameters of Si such as channel thickness and strain therein. It is revealed that the process of smoothing $\text{Si}_{1-x}\text{Ge}_x$ virtual substrates via Chemical Mechanical Polishing (CMP) had almost no impact on mobility characteristics of n- and p-channel. However, changing the Ge concentration in both the virtual substrate and compressively strained channel in the double-heterostructure with optimized layer thicknesses resulted in maximum hole mobility enhancements [37].

Another detailed discussion on sSi p-MOSFETs investigates the effect of channel thickness and larger strain values in the Si channel [38] and the consequences of increasing the Ge concentration in relaxed $\text{Si}_{1-x}\text{Ge}_x$ buffers to values up to $x = 0.5$. It is discussed that much higher hole mobility enhancements took place than previously reported [38] in sSi

single heterostructures. The important feature of direct bonding of sSi with an insulating substrate to create strained SOI(sSOI) [39, 40] was that the relaxed $\text{Si}_{1-x}\text{Ge}_x$ layer could be taken off while still maintaining the high strain in the Si layer.

REFERENCES:

1. M. leong, B. Doris, J. Kedzierski, K. Rim and M. Yang, *Science*, 306(5704) (2004) 2057.
2. A. R. Khan, J. Stangl, G. Bauer, D. Buca, B. Holländer, H. Trinkaus, S. Mantl, R. Loo and M. Caymax, *Semicond. Sci. Technol.*, 22 (2007) S212.
3. D. A. Antoniadis, *Symposium on VLSI Technology Digest of Technical Papers*, (2002) 2.
4. R. People, J. C. Bean, D. V. Lang, A. M. Sergent, H. L. Störmer, K. W. Wecht, R. T. Lynch and K. Baldwin *Appl. Phys. Lett.*, 45(11) (1984) 1231.
5. R. People and J. C. Bean, *Appl. Phys. Lett.*, 48(8) (1986) 538.
6. H. M. Manasevit, I. S. Gergis and A. B. Jones, *Appl. Phys. Lett.*, 41(5) (1982) 464.
7. G. Abstreiter, H. Brugger and T. Wolf, *Phys. Rev. Lett.*, 54(22) (1985) 2441.
8. G. Schuberth, F. Schäffler, M. Besson, G. Abstreiter and E. Gornik, *Appl. Phys. Lett.*, 59(25) (1991) 3318.
9. K. Ismail, B. S. Meyerson and P. J. Wang, *Appl. Phys. Lett.*, 58(19) (1991) 2117.
10. G. L. Patton, S. S. Iyer, S. L. Delage, S. Tiwari and J. M. C. Stork, *IEEE Electron Device Letters*, 9(4) (1988) 165.
11. D. K. Nayak, J. C. S. Woo, J. S. Park, K. Wang and K. P. MacWilliams, *IEEE Electron Device Letters*, 12(4) (1991) 154.
12. S. Verdonckt-Vandebroek, E. F. Crabbe, B. S. Meyerson, D. L. Hareme, P. J. Restle, J. M. C. Stork, A. C. Megdanis, C. L. Stanis, A. A. Bright, G. M. W. Kroesen and A. C. Warren, *Device Letters, IEEE*, 12(8) (1991) 447.

13. Y. H. Luo, J. L. Liu, G. Jin, J. Wan and K. L. Wang, *Appl. Phys. A: Mater. Sci. Process.*, 74 (2002) 699.
14. K. K. Linder, K. K. Linder, F. C. Zhang, J.-S. Rieh, P. Bhattacharya and D. Houghton, *Appl. Phys. Lett.*, 70 (1997) 3224.
15. H. Yin, K. D. Hobart, F. J. Kub, S. R. Shieh, T. S. Duffy and J. C. Sturm, *Appl. Phys. Lett.*, 82 (2003) 3853.
16. E. A. Fitzgerald, *Materials Science Reports*, 7(3) (1991) 87.
17. E. A. Fitzgerald, A. Y. Kim, M. T. Currie, T. A. Langdo, G. Taraschi and M. T. Bulsara, *Materials Science and Engineering B*, 67(1-2) (1999) 53.
18. R. Hull and J. C. Bean, *Critical Reviews in Solid State & Materials Sciences*, 17(6) (1992) 507.
19. K. Ismail, B. S. Meyerson, S. Rishton, J. Chu, S. Nelson and J. Nocera, *IEEE Electron Device Letters*, 13(5) (1992) 229.
20. U. Konig, A. J. Boers, F. Schaffler and E. Kasper, *Electronics Letters*, 28(2) (1992) 160.
21. U. Konig and F. Schaffler, *Electronics Letters*, 27(16) (1991) 1405.
22. J. Welser, J. L. Hoyt and J. F. Gibbons, *International Electron Devices Meeting*, (1992) 1000.
23. J. Welser, J. L. Hoyt and J. F. Gibbons, *IEEE Electron Device Letters*, 15(3) (1994) 100.
24. D. K. Nayak, J. C. S. Woo, J. S. Park, K. L. Wang and K. P. MacWilliams, *Appl. Phys. Lett.*, 62(22) (1993) 2853.
25. Y. H. Xie, Don Monroe, E. A. Fitzgerald, P. J. Silverman, F. A. Thiel and G. P. Watson, *Appl. Phys. Lett.*, 63(16) (1993) 2263.
26. U. Konig and F. Schaffler, *IEEE Electron Device Letters*, 14(4) (1993) 205.
27. K. Ismail, J. O. Chu and B. S. Meyerson, *Appl. Phys. Lett.*, 64(23) (1994) 3124.
28. K. Rim, J. L. Hoyt and J. F. Gibbons, *Electron Devices Meeting*, (1995) 517.
29. D. K. Nayak, K. Goto, A. Yutani, J. Murota and Y. Shiraki, *IEEE Transactions on Electron Devices*, 43(10) (1996) 1709.

30. G. Höck, E. Kohn, C. Rosenblad, H. von Känel, H.-J. Herzog and U. König, *Appl. Phys. Lett.*, 76(26) (2000) 3920.
31. M. Arafa, K. Ismail, P. Fay, J.O. Chu, B.S. Meyerson and I. Adesida, *Electronics Letters*, 31(8) (1995) 680.
32. M. Arafa, P. Fay, K. Ismail, J.O. Chu, B.S. Meyerson and I. Adesida, *IEEE Electron Device Letters*, 17(3) (1996) 124.
33. L. J. Huang, J. O. Chu, D. F. Canaperi, C. P. D'Emic, R. M. Anderson, S. J. Koester and H.-S. Philip Wong, *Appl. Phys. Lett.*, 78(9) (2001) 1267.
34. G. Taraschi T. A. Langdo, M. T. Currie, E. A. Fitzgerald and D. A. Antoniadis, *Journal of Vacuum Science & Technology B: Microelectronics and Nanometer Structures*, 20(2) (2002) 725.
35. Z. Y. Cheng, M.T. Currie, C.W. Leitz, G. Taraschi, E. A. Fitzgerald, J. L. Hoyt and D.A. Antoniadis, *IEEE Electron Device Letters*, 22(7) (2001) 321.
36. T. Tezuka, N. Sugiyama and S. Takagi, *Appl. Phys. Lett.*, 79(12) (2001) 1798.
37. C. W. Leitz, M. T. Currie, M. L. Lee, Z.-Y. Cheng, D. A. Antoniadis and E. A. Fitzgerald, *Appl. Phys. Lett.*, 79(25) (2001) 4246.
38. C. W. Leitz, M. T. Currie, M. L. Lee, Z.-Y. Cheng, D. A. Antoniadis and E. A. Fitzgerald, *Journal of Applied Physics*, 92(7) (2002) 3745.
39. T. A. Langdo, M. T. Currie, A. Lochtefeld, R. Hammond, J. A. Carlin, M. Erdtmann, G. Braithwaite, V. K. Yang, C. J. Vineis, H. Badawi and M. T. Bulsara, *Appl. Phys. Lett.*, 82 (24) (2003) 4256.
40. T. S. Drake, C. Ní Chléirigh, M. L. Lee, A. J. Pitera, E. A. Fitzgerald, D. A. Antoniadis, D. H. Anjum, J. Li, R. Hull, N. Klymko and J. L. Hoyt, *Appl. Phys. Lett.*, 83(5) (2003) 875.

X-RAY DIFFRACTION ANALYSIS OF Si/SiGe RESONANT TUNNELING STRUCTURES

A. R. KHAN^{1*}, M. MEDUÑA¹, G. BAUER¹,
C. FALUB² AND D. GRUETZMACHER²

¹Institut for Semiconductor and Solid State Physics, University of Linz, A-4040 Linz, Austria

²Paul Scherrer Institut, CH-5232 Villigen, Switzerland

Corresponding Author: aaliya.rehman@gmail.com

(Received: September 23, 2010)

ABSTRACT: Resonant tunneling diodes have been fabricated using strained-Si wells and strained Si_{0.6}Ge_{0.4} barriers on a relaxed Si_{0.8}Ge_{0.2} *n*-type substrate, designed to demonstrate negative differential resistance. The analysis of the diffraction data obtained, using synchrotron facility, has been simulated using a standard matrix approach for calculating conventional diffraction from multilayers.

Keywords: X-ray diffraction; semi-conductors; bi-axial strain

1. INTRODUCTION

The development of specified applications like high frequency oscillator or high speed switching are based on resonant tunneling diode (RTD) [1,2]. Recent improvement in epitaxial growth technology of Si-based group IV semiconductor has enabled the formation of high quality RTD structures [3]. Previously, p-type RTDs with Si/strained Si_{0.6}Ge_{0.4} heterostructures on Si(100) were fabricated, and sharp current peaks were observed [4,5]. However, obvious crystallinity degradation resulted in lowering of reproducibility. Further revised fabrication processes which varied parameters (e.g., Ge fraction and growth temperature) and improved crystallinity were achieved for high quality RTDs [5]. In this paper we present an X-ray study of SiGe heterostructures on SiGe (20%) substrate prepared for resonant tunneling diodes.

2. METHOD

The samples consist of a sequence of 15 SiGe and Si layers grown pseudomorphically on top of a relaxed SiGe buffer (Fig. 1). These layers form a resonant tunneling diode (RTD). From reciprocal space maps, we obtain information on the composition and the strain state of the buffer layers.

We have investigated the resonant tunneling structures samples consisting of a SiGe (40%) quantum well separated by a Si barrier where the individual samples differ from each other by the thickness of SiGe well and Si barrier.

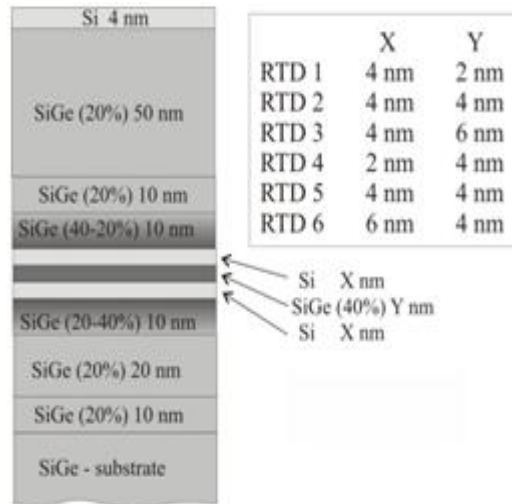


Fig.1: Schematic view of the structure for samples grown on the SiGe (20%) substrate.

The three-layer structure is strain-symmetrized by the graded region (SiGe 20-40%) below and above the structure. The whole structure is grown on the SiGe (20%) pseudosubstrate. The schematic sketch of the sample structure is in Fig. 1. The samples were characterized by AFM, x-ray diffraction and x-ray reflectivity measurements, performed in laboratory at University of Linz and at synchrotron source at HASYLAB in Hamburg.

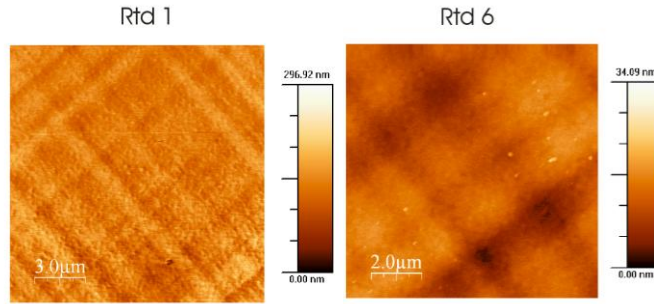


Fig. 2: AFM viewgraphs for samples RTD 1 and 6.

In order to get information on the quality of the sample surface and the surface morphology, we have performed the AFM topography images of the sample surfaces. Figure 2 shows an example of AFM topography of two of the samples. All AFM figures showed the presence of cross-hatch patterns on all samples, indicative of the fact that through the growth of step-graded buffer layer strain relaxation occurs.

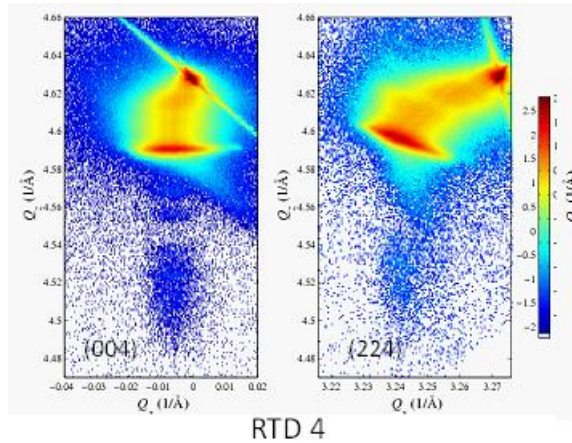


Fig.3: Examples of XRD reciprocal space maps around the (004) and (224) for samples RTD 4 one of the selected azimuths.

Nevertheless from diffraction x-ray reciprocal space maps it is seen that in all samples the layers on top of the graded buffer are pseudomorphically strained to this buffer layer (Fig. 3).

Since the scattered intensities from the structure including the SiGe well and Si barrier are very low in the RSM measurements at the rotating anode

set-up in Linz, we have used only the diffraction peak position in the $Q_x Q_z$ space for the strain analysis of the structure. The position of the peaks in the Q-space allows us to estimate the average lattice parameter of the layers in the investigated structure.

3. RESULTS AND DISCUSSION

We have found that the measurements of the samples RTD 4 and RTD 6 exhibit the significant diffraction maximum at the position $Q_z=4.524 \text{ 1/\AA}$ corresponding to the average Ge content 42% in SiGe, but the measurements of the samples RTD 1, RTD 2, RTD 3 and RTD 5 show a peak at $Q_z=4.555 \text{ 1/\AA}$ corresponding to the average Ge content of 33% in SiGe layer. From this follows that samples RTD 4 and RTD 6 are very close to the nominal values from the growth protocol. All results obtained from the diffraction data are shown in Table I. The data given in Table I are the average plane lattice constant $a_{||}^L$, the lattice constant along growth direction a_{vert}^L , the Ge content x_{Ge} and the in-plane strain value $\varepsilon_{||}$ with respect to a SiGe bulk material of equal Ge content).

In order to see a detailed profile of the peaks and oscillations originating from the tunneling structure in 004 and 224 diffraction, we have performed a synchrotron measurement of corresponding Q_z scans. The measurements together with the simulations are shown in the angular space (ω incidence angle) in Figure 4.

The diffraction data have been simulated using a standard matrix approach for calculating conventional diffraction from multilayers [6]. For the simulations, we have used a model with nominal structural parameters, where the graded region was substituted by a set of steps in Ge content. Only the thickness of SiGe well and Si barrier together with their lattice parameters were used as fitting parameters.

Table I. Nominal and diffraction sample parameters

Sample Name	comment	aver. $a_{ }^L$	aver. a_{vert}^L	x_{Ge}	$\varepsilon_{ }$	R
RTD 1	graded buffer	5.474	5.474	21%	-0.0001	0.99
	SiGe(40%) layer	5.474	5.516	32%	0.0044	0.64

RTD 2	graded buffer	5.472	5.474	21%	0.0004	0.97
	SiGe(40%) layer	5.472	5.520	33%	0.0059	0.60
RTD 3	graded buffer	5.472	5.474	21%	-0.0002	0.95
	SiGe(40%) layer	5.472	5.519	33%	0.0049	0.58
RTD 4	graded buffer	5.471	5.474	20%	0.0003	0.96
	SiGe(40%) layer	5.471	5.555	42%	0.0087	0.45
RTD 5	graded buffer	5.471	5.475	20%	0.0004	0.95
	SiGe(40%) layer	5.471	5.517	32%	0.0047	0.60
RTD 6	graded buffer	5.471	5.475	20%	0.0004	0.95
	SiGe(40%) layer	5.472	5.554	42%	0.0084	0.47

Thus we could obtain an estimate of the Ge content in the SiGe wells and the Si barriers. The layer parameters used for simulations, which are different from the nominal values are shown together with the simulations in Figure 4.

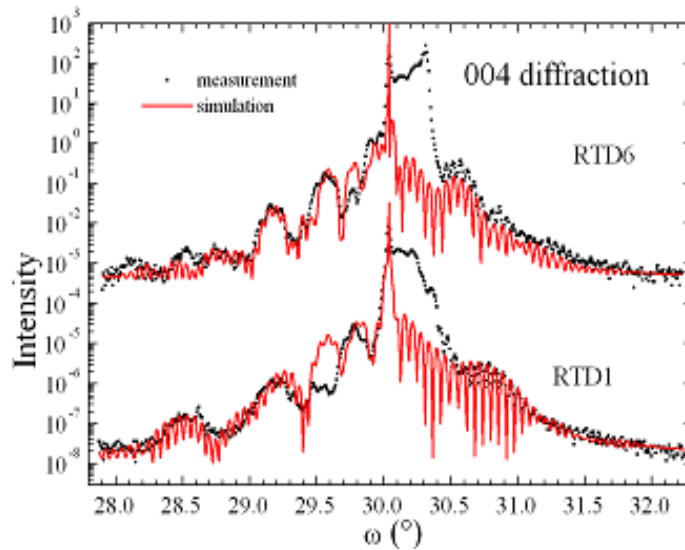


Fig.4: Simulations of XRD (004) and (224) scans.

In the simulations, we have fixed the Ge content in SiGe well to 40% and varied the layer thicknesses and small Ge content in Si barrier, which might be present due to interdiffusion in such thin layers. As the diffraction simulations show, the sample RTD 6 and RTD 1 seem to have larger thickness of the upper Si barriers than expected but the Ge content most likely corresponds to the nominal values. On the other hand, the diffraction simulations still do not correspond very well to the measured data, may be due to the fact that the model used in the evaluation process is still not sufficient for the description of sample structure.

REFERENCES

1. M. Sweeny, *Appl. Phys. Lett.*, **54** (1989) 546.
2. D. J. Day, *Appl. Phys. Lett.*, **57** (1990) 1260.
3. U. Gennser, *J. of Vac. Sci. & Tech. B: Microelectronics and Nanometer Structures*, **8** (1990) 210.
4. K. Ismail, *Appl. Phys. Lett.*, **59** (1991) 973.
5. J. R. Söderström, *Appl. Phys. Lett.*, **55** (1989) 1094.
6. Ullrich Pietsch, V. Holy and T Baumbach, *High-Resolution X-Ray Diffraction: from Thin Films and Multilayers*, Springer-Verlag, Berlin, (1999).

JOURNAL OF NATURAL SCIENCES AND MATHEMATICS

INFORMATION FOR AUTHORS

1. TYPES OF PAPERS ACCEPTED

The Journal aims at publishing original research papers and the review papers from distinguished scientists on Mathematics, Physics, Chemistry and Computer Science.

2. SUBMISSION OF MANUSCRIPTS

Manuscripts should be submitted in duplicate to the Section Editor concerned. All papers are refereed. The decision of the Editorial Board regarding the acceptance and publication of the paper will be final.

3. PREPARATION OF MANUSCRIPT

3.1 Language and Style

All submissions should be in English, typed in double spacing on one side of the paper only with a left hand margin of at least 4 cm. Mathematical expressions must be carefully printed. Computer composed manuscript on C.D. in Microsoft Word is required for speedy publication.

3.2 Abstract

This should comprise a brief and factual summary of contents and should be suitable for direct use by abstracting journals. This will seldom require more than 200 words.

3.3 Section/Sub-Section Headings

Papers should be divided into sections / sub-sections and numbered as exemplified in the headings of this INFORMATION FOR AUTHORS.

3.4 References

References should be numbered consecutively in the text, e.g. "According to a recent theory [6]...it is well established [7]" and collected at the end of the paper in following style:

6. I. M. Ghauri and P. Feltham, J. Nat. Sci. Math., 26 (1986) 63.

7. W. Greiner and J. Maruhn, Nuclear Models, Springer-Verlag, Berlin, (1996).

3.5 Illustrations

Line diagrams must be drawn in black ink on white paper; original and two copies are required. Photographs or half-tone reproduction should be in the form of highly glazed prints. A separate list of captions for illustrations should be provided.

4. PROOFS

Only one set of proof is sent to the authors for correction.

CONTENTS

Sr. No.	TITLE	PAGE
1.	AMINO ACID ANALYSIS USING ION EXCHANGE RESINS A. S. KHAN AND F. FAIZ	01
2.	FUNDAMENTAL GROUP OF THE DYNAMICAL GRAPH M. EL-GHOUL AND M. A. EL-FATTAH	19
3.	ON s^* -CLOSED SETS AND s^* -NORMAL SPACES M. KHAN, T. NOIRI AND M. HUSSAIN	31
4.	THE EFFECT OF FLUORINE DOPING ON OPTOELECTRONIC PROPERTIES OF TIN-DIOXIDE (F: SnO ₂) THIN FILMS S. A. YOUSAF AND S. ALI	43
5.	EFFECT OF PARTICLE SIZE ON THE STRUCTURAL AND TRANSPORT PROPERTIES OF La _{0.67} Ca _{0.33} MnO ₃ NANOPARTICLES M. Z. IQBAL, S. ALI AND M. A. MIRZA	51
6.	VARIATION OF ION ENERGY FLUX WITH INCREASING WORKING GAS PRESSURES USING FARADAY CUP IN PLASMA FOCUS DEVICE H. A. R. TARIQ, I. A. KHAN, U. IKHLAQ AND A. HUSSAIN	65
7.	UNIAXIALLY STRAINED Si/SiGe HETEROSTRUCTURES A. R. KHAN	73
8.	X-RAY DIFFRACTION ANALYSIS OF Si/SiGe RESONANT TUNNELING STRUCTURES A. R. KHAN, M. MEDUÑA, G. BAUER, C. FALUB AND D. GRUETZMACHER	81